DEVELOPMENT OF RAILTRACK TUNED MASS DAMPER MODULE

TAM PO LAI

M.Phil

The Hong Kong Polytechnic University

2018

The Hong Kong Polytechnic University

Department of Applied Physics

Development of Railtrack Tuned Mass Damper Module

TAM Po Lai

A thesis submitted in partial fulfillment of the requirements

for the degree of Master of Philosophy

March 2017

THE HONG KONG POLYTECHNIC UNIVERSITY

Certificate of Originality

I hereby declare that this thesis is my own work and that, to the best of my knowledge and belief, it reproduces no material previously published or written, nor material that has been accepted for the award of any other degree or diploma, except where due acknowledgement has been made in the text.

_____ (Signature)

TAM Po Lai (Name of candidate)

Abstract

Among all six types of railway noise, rolling noise is the dominant noise in most of the speed range. Wheel/rail interaction induces wheel and rail vibrations which makes rolling noise, and such interaction also excites a pinned-pinned mode of vibration which frequency depends on the sleeper spacing.

For UIC60 and UIC54 rail track, our on-site measurements, together with finite elements analysis, showed that the pin-pin resonance modes of the rail track in lateral and vertical direction (i.e. the two principal directions perpendicular to the length of rail tracks) are in the frequency ratio of around 1:2. Following our recent development of Tuned Mass Damper(TMD), multiple masses were employed so that they oscillate along the shear direction of the resilient layers to form a multiple spring-mass system in both vertical and lateral directions. As the damping mechanism strongly relies on the stiffness of the resilient layer, thus a resilient composite material with orthogonal shear moduli in orthogonal directions can be used to tackle the issue of different pin-pin resonance modes in both lateral and vertical directions. Since the resonant frequency is proportional to the square root of the modulus, with a frequency ratio of ~ 2 between the vertical and lateral pin-pin resonance modes, a ratio of 4 between the shear moduli of the two respective directions is required.

In this study, aligned glass fibres and copper fibres were embedded into silicone matrix to form uniform composite resilient layers with different orthogonal shear moduli. Their shear stiffness were measured by a tensile tester, with the setup for shear modulus measurement based on the International Organization for Standardization ISO-1827. Our results showed that these composites obtained an acceptable orthogonal shear moduli

ratio. Vibration tests were performed to verify that two natural frequencies were observed in these TMDs using the orthogonal resilient layers, which is not possible for TMDs using homogeneous resilient layer materials. Hence, resilient layer material of orthogonal shear moduli as applied on the TMD is promising for suppressing the two directions pinned-pinned resonance modes in rail tracks. Meanwhile, a finite element analysis was introduced to investigate the optimal arrangement of the composite.

List of Publication

1. **Po-lai Tam**, Chi-wah Leung, Chee-leung Mak, Wilson Ho and Ting Cai, "Development of orthogonal resilient materials for Tuned Mass Damper", *The 12th International Workshop on Railway Noise (IWRN12)*, 2016

Acknowledgement

First, I would like to express my appreciation and thank my chief supervisor Dr. MAK Chee Leung and co-supervisor Dr. LEUNG Chi Wah for the valuable and timely guidance. I have always been delighted by their advices whenever I was being hesitated. The whole research project has been improved by their advice and comments.

Also, I would like to show my gratitude to Mr. Wilson HO and Mr. CAI Ting, from Wilson Acoustic Limited, for giving me a precious opportunity to work on an interesting and exciting research project. Not only industrial knowledge and experience they have given me, but also the insistence and determination towards research and development that always amaze me.

I would like to show my sincere gratitude to all my officemates, Mr. LEE Kai Fung, Mr. TAN Choon Kiat, Mr. TING Ho Fung and Mr. WONG Wang Cheung for their encouragement, suggestions and inspiration on the study. I would like to acknowledge Mr. WONG Hon Fai and Ms. NG Sheung Mai for the motivation and assistance.

Finally, I would like to thank my family for their support and patience, and Ms YIP Hoi Ting for her love, patience and constant support.

This work is supported by the Innovation and Technology Fund, HKSAR through the Teaching Company Scheme (UIT/128). This support is gratefully acknowledged.

This research would never be completed without any crucial and essential parties above.

Any opinions, findings, conclusions or recommendations expressed in this material do not reflect the views of the Government of HKSAR or the Innovation and Technology Commission.

Table of Contents

List of Figures

List of Tables

1. Introduction

Railway networks have been broadly adopted for express mass transportations alongside with the expansion of cities, including Hong Kong. Together with vibrations, the noise generated by railways becomes a growing environmental concern to the residents beside the network and passengers on trains. Railway networks are building closer to the residential areas and the noise impact to the residents draws more attractions than ever. Substantial regulations have been setup in cities in order to suppress the noise influence down to acceptable levels.

Railway noise can be divided into six types, which are rolling noise, curve squeal, bridge noise, aerodynamic noise, traction noise and ground-borne noise.

Rolling noise is the dominant source in most speed range, however, rolling noise increases with train speed V at a rate of around $30\log_{10}V$[1]. The cause of rolling noise is from the interaction between wheel and rail. Vertical vibration between wheel and rail is induced by the interaction on wheel's rough running surface and rail, rolling noise emission of the vibrating wheel and rail. Thus, roughness on running surface and pin-pin resonance vibration are crucial factors to rolling noise. This thesis will focus on rolling noise and further discussion in 1.1.

Traction noise is considerably less speed-dependent, and thus is often dominant at low speed. It is from traction motor and fans, and from engines, intake and exhaust, etc.

Aerodynamic noise is greatly dependent on train speed, therefore, it is a dominant source at high speed. Aerodynamic noise is caused by unsteady air flow over the train, and can be broadband or tonal noise.

Similarly, the interaction between wheel and rail causes curve squeal, however, with different component. Curve squeal excited by transverse forces at the interaction occurring between wheel and rail during curving. It is associated with the vibration of the wheel in its one of resonance mode, therefore, it is greatly tonal.

Bridge noise emits when a train travels over a bridge, and the noise characteristics heavily depends on the type of bridge. A dynamic force acting on the bridge from the railtrack produces bridge noise. Most of the bridge noise is emitted at low frequency range.

Ground-borne vibration transmits over two methods: firstly, the low frequency vibration about 2 - 80 Hz often associates with freight trains; secondly, trains passage in tunnel in urban area or surface railways excite structural surface of rooms that vibrate in higher frequency at about 30 – 250Hz. Then the structure surface will radiate low frequency noise [1].

To reduce undesirable noise and vibration on the rail track, Wilson Acoustics Limited developed a tuned mass damper (TMD). Studies showed that this TMD reduces noise level during traffic pass by and suppresses the growth of corrugation, which is a kind of regular roughness on the running surface of rail[2, 3]. In current design, multiple masses and resilient layers are employed in an interleave method shown in Figure 1. The oscillation masses are designated to oscillate along their shear direction to the resilient layers, forming a mass-spring system in both vertical and lateral directions to work as a damper. Each mass and resilient layers set can only be tuned for single frequency. However, the rail has different pinned-pinned resonance modes between vertical and lateral direction due to the profile of rail. Among the common types of railtrack, the frequency ratio in lateral and vertical direction is about 1:2[1]. The resilient layers are required to have a shear stiffness ratio of 1:4, because the resonant frequency is

proportional to the square root of shear modulus. Therefore, a resilient layer with orthogonal feature is required to handle vertical and lateral pinned-pinned resonance modes for single mass.

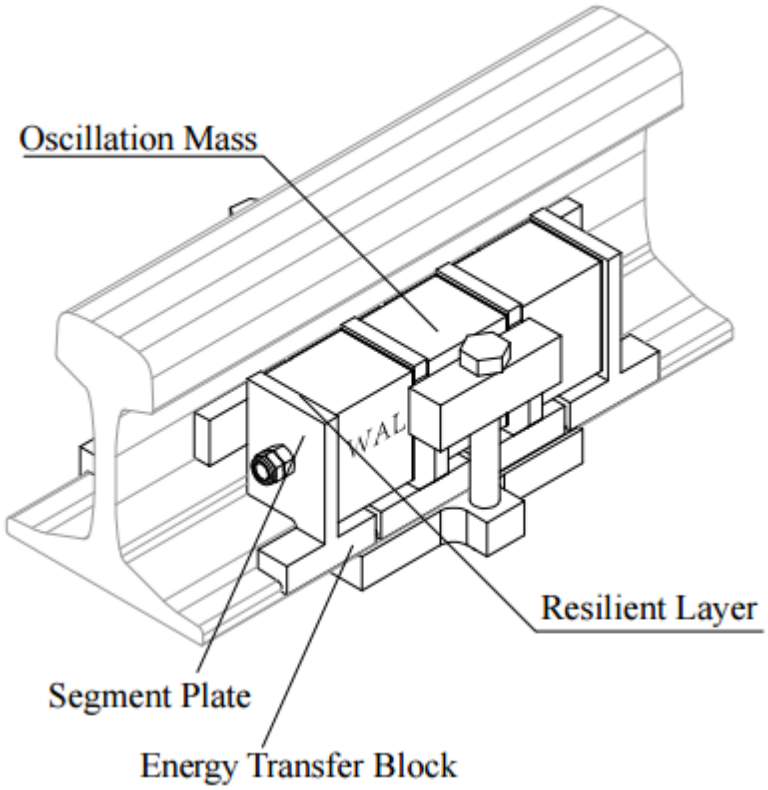

Figure 1. Current design of Multi-directional tuned mass damper (MDTMD)

1.1. Introduction to Rolling Noise

The interaction of the wheel and rail generates rolling noise, both wheel and rail radiate a great portion of the noise. General speaking, the wheel and railtrack are not totally smooth, their roughness induces frictional interaction between each other. This interaction causes vibration on the wheel or rail, primarily in vertical direction. Consider the movement of the wheel as a wave with a wavelength λ, and the wheel travels at a speed V (same as the speed of train). Then, the propagated wave has a frequency f given by,

$$f = \frac{V}{\lambda}$$ **Equation 1**

The resultant vibration frequency from wheel/rail interaction is proportional to the speed of train V and inversely proportional to the wavelength of roughness λ. The wavelength of the roughness refers to the distance over the periodic wear pattern. The vibrations in high frequency range are transmitted into both the wheel and railtrack, and these vibrations radiate noise from the structures into air.

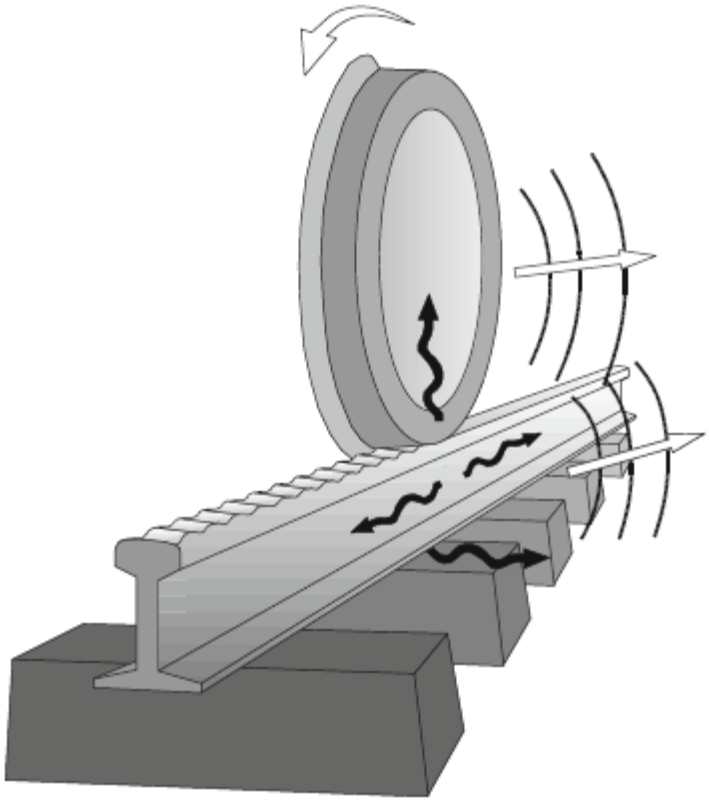

Figure 2. Illustration of the mechanism of generation of rolling noise[1]

The whole process of rolling noise generation can be summarized in the flowchart as shown in Figure 3. Both roughnesses on wheel and rail running surface activate vertical vibrations of the wheel and rail structure while the train passing by the spot, the vibrations of wheel and rail induce radiation of sound.- Hence, all sounds emitted from wheel and rail integrates into rolling noise[1].

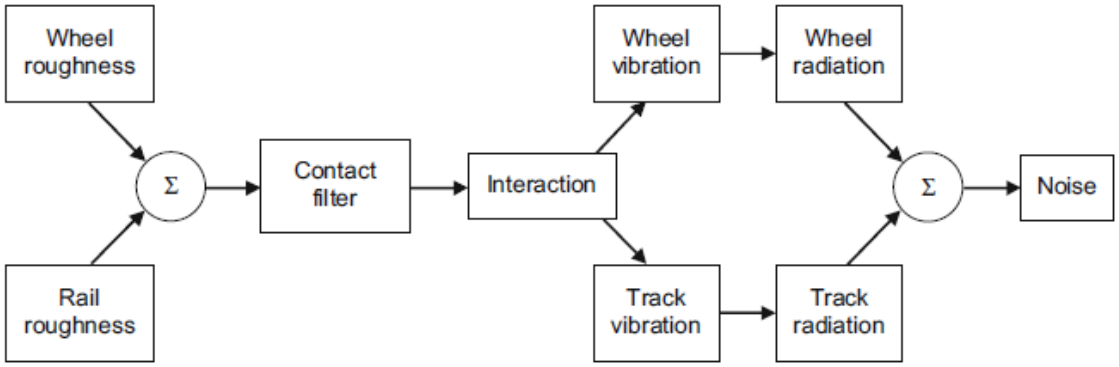

Figure 3. Flowchart of rolling noise generation[1]

Rolling noise is mainly induced by vertical vibration from wheel/rail interaction, while squeal noise is also induced by wheel/rail interaction but in lateral direction. This type of noise occurs at bending section, especially tight bend, so it is also called curve squeal. The noise is initiated by unsteady transverse forces at the contact in bending, the excitation is due to stick-slip behaviour between wheel and rail, i.e., top-of-rail squeal that lateral creepage at the contact between the wheel and top of the rail head, flange squeal that wheel flange rubbing on the inner rail head surface. These squeals excite wheel or rail harmonics, therefore, squeal noise is usually strongly tonal[1].

1.1.1 Roughness on railtrack

Figure 4. Significant roughness on railtrack, taken on-site measurement (July 2015, nearby Quarry Bay station).

The surface unevenness is commonly referred to as “roughness”, the wavelengths of roughness of 5 - 500mm produce rolling noise. Although macro-roughness (of larger than a millimetre) is directly related to rolling noise, micro-roughness (of a millimetre or less) is necessary for traction and braking[1].

Figure 5. CAT in use[4].

The rail profile height reflects the roughness on the railtrack within the section, it can be measured through a corrugation analysis trolley (CAT) as shown in Figure 5. CAT measures the rail profile by contact measurement that trolley goes through the whole section of the railtrack to acquire data. The data results from CAT will be displayed in micrometre to show the rail profile height of the corresponding location, the higher the value means the more serious roughness on track as indicated in Figure 6. In the alternative, data can be converted into roughness level based on a reference level 1μm against wavelength of roughness or frequency at certain speed as displayed in Figure 7. The conversion between wavelength of roughness and the frequency at certain speed is referred to Equation 1[1, 4].

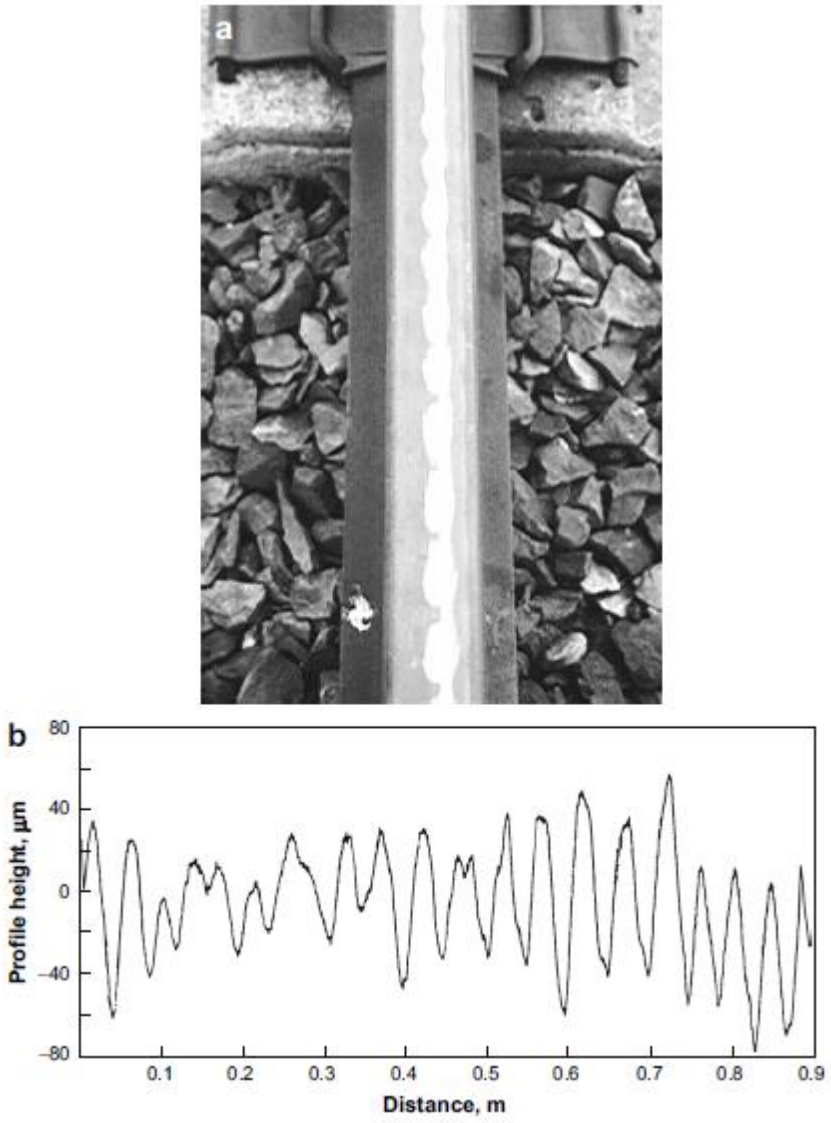

Figure 6. (a) A photo of rail corrugation and (b) a measured rail profile height at the same location[1].

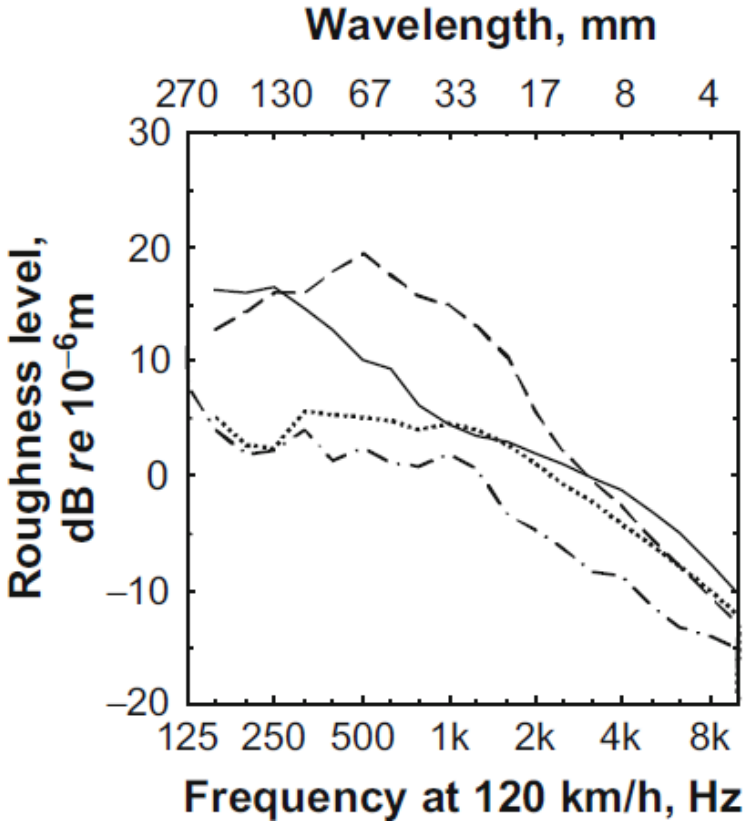

Figure 7. A typical roughness against wavelength and frequency at train speed of 120km/h[1].

1.1.2 Pinned-pinned Resonance

Pinned-pinned resonance mode is a railtrack vibration that occurs between two consecutive sleepers. Consider the railtrack as a beam that is fixed at sleepers or rail fastening, the source of initial excitation is the wheel/rail interaction during the train pass-by. The frequency of pinned-pinned resonance primarily depends on the sleeper spacing and track cross-section profile, which is given by

$$f = \frac{\pi}{2L^2}\sqrt{\frac{EI}{m}}\left[1-\frac{1}{2}\left(\frac{\pi r_g}{L}\right)^2\left(1+\frac{2(1+\upsilon)}{\mathrm{K}}\right)\right]$$

Equation 2

where in, m is the rail's mass per unit length
EI is the rail's bending stiffness
L is the sleeper spacing
r_g is the radius of gyration
K is the shear constant of the cross section
v is the rail's passion ratio

Since the sleeper separation is usually regular in certain section, the railtrack shares the same frequency of pinned-pinned resonance. In this case, the same mode of resonance propagates along the railtrack, and accumulates in the railtrack. Due to the constant wear with wheel under particular frequency, there is a periodic or quasi-periodic wear pattern appears on the running surface of the railtrack, which is called corrugation. The corrugation will induce a more intense interaction and make a stronger vibration, then this results a higher noise level[1, 4].

Figure 8. Pinned-pinned resonance corrugation on the rail[4]

According to the previous on-site measurement, an UIC60 railtrack with sleeper separation of 0.7m has vertical and lateral pinned-pinned resonance modes in different frequencies. Refer to the mobility spectra as shown in Figure 9, the peak at around 800Hz is a vertical pinned-pinned mode. Figure 10 shows the lateral mobility spectrum

measurement. In the figure, a peak identified at around 400Hz is observed. It should be noted that mobility is the ratio of the velocity-response at a point to the excitation force at specific point, the measurement involved a force hammer to measure the excitation force and trigger the data logger connected with accelerometers to measure the response of the rail in certain points[5]. Thus, based on Figure 9 and Figure 10, it is noticed that the resonance modes have a ratio of 1:2.

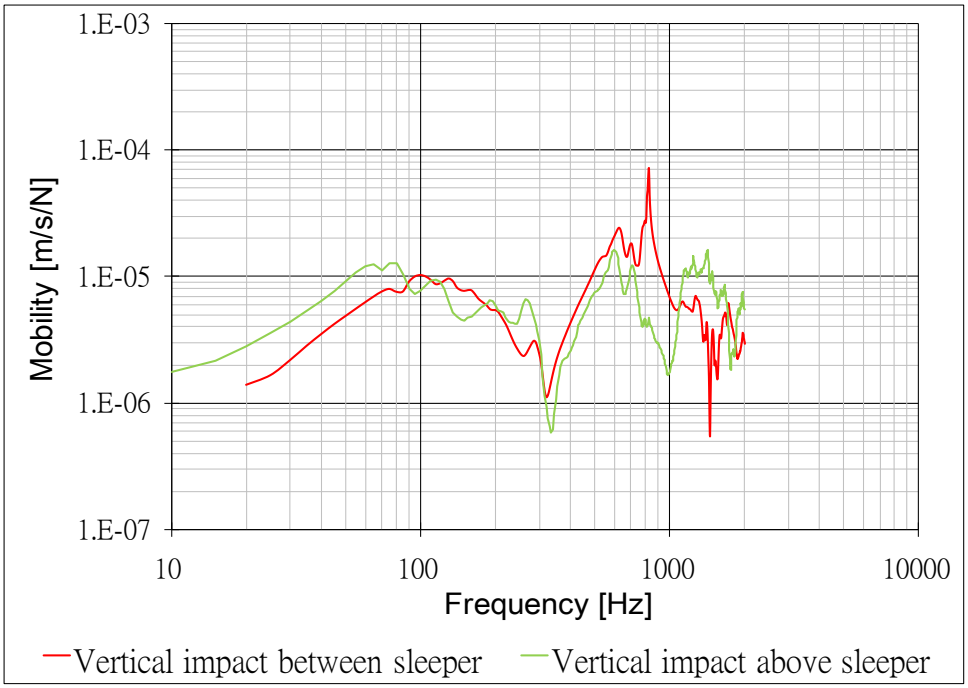

Figure 9. Mobility spectrum under vertical impact

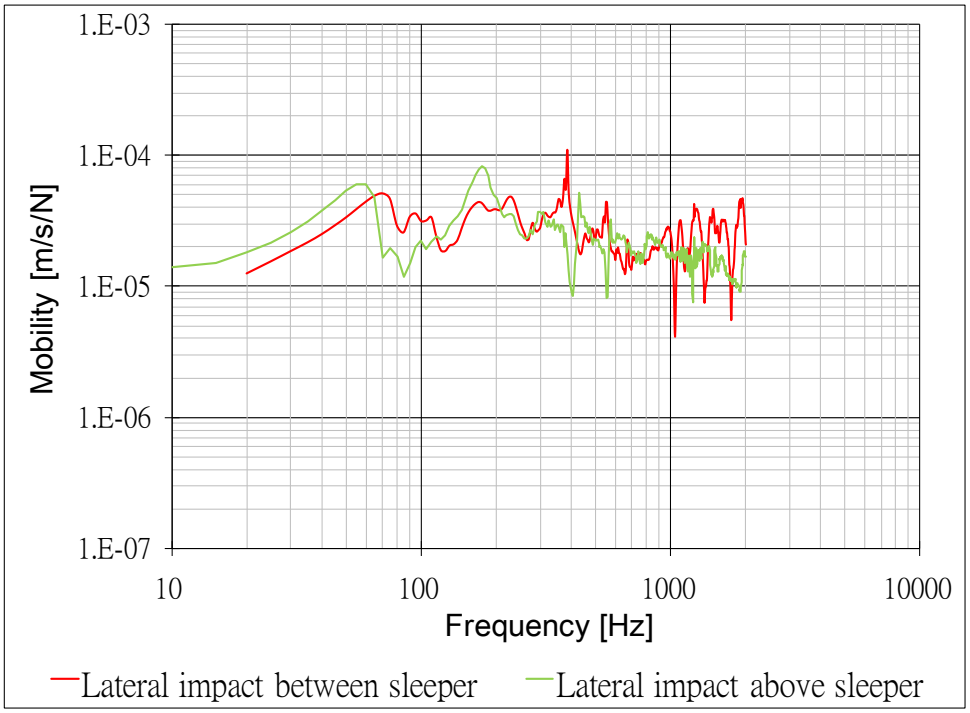

Figure 10. Mobility spectrum under lateral impact

Pinned-pinned resonance corrugation mainly occurs in straight track or gentle curve with minimal flange contact, and train with heavy loading will induce a stronger corrugation. A heavy corrugation on rail's running surface can be easily observed by naked eyes, which is shown in Figure 8. Otherwise, a CAT is adopted to extract a more detailed measurement, i.e. a peak at roughness in the spectrum. The corrugation can be reduced by rail grinding when the corrugation grows to a certain level. Indeed, studies show that a tuned mass damper is able to reduce the corrugation growth[3, 4, 6].

1.2. Principle of Tuned Mass Damper

A tuned mass damper (TMD) is a passive device that mounted to a structure with the aim of reducing the dynamic response, mainly tonal vibration, of the structure. A TMD consists of a mass, a spring and a damper that is tuned to a specific structural frequency. The damper system will resonate in an out of phase condition with the structure when the

frequency is excited. The vibration energy is dissipated by the damper module inertia acting on the structure[7, 8].

The tonal vibration refers to a phenomenon called resonance. When a periodic response is excited by a periodic loading to a structure, for example a rotating machinery mounted on the floor when the rotating masses are unbalance. If the force oscillation matches one of the resonance frequencies of the structure, the magnitude of displacement, velocity and acceleration will be excessive. A mass damper with appropriate value of stiffness and damping is able to avoid resonance[7].

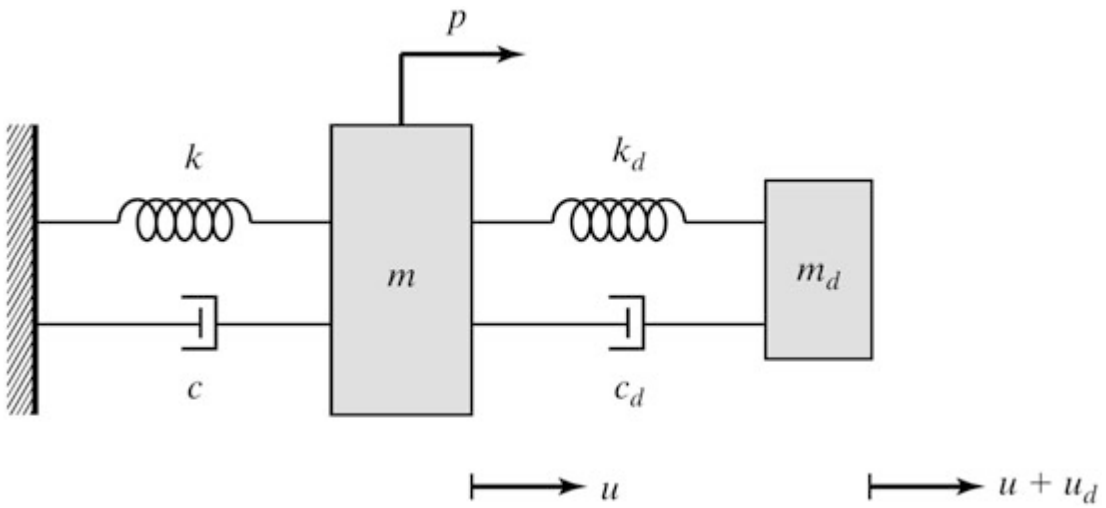

Figure 11. Single degree of freedom – Tuned mass damper system[7]

In Figure 11, the idea of the tuned mass damper system is illustrated through the two-mass system. The parameters with subscript *d* refer to the tuned mass damper system and the parameters without subscript refer to the primary mass (structure), where *k* is the spring constant, *c* is the damping coefficient, *m* is the mass and *u* is the displacement from the equilibrium position. The system is simplified as a single degree of freedom system. [7, 9]

Angular frequency of the primary mass is given by:

$$\omega = \sqrt{\frac{k}{m}} \qquad \textbf{Equation 3}$$

The damping coefficient of the primary mass *c* is given by:

$$c = 2\xi\omega m \qquad \textbf{Equation 4}$$

where ζ is the damping ratio, a ratio of actual damping to critical damping to the system.

Similarly, angular frequency of the tuned mass is given by:

$$\omega_d = \sqrt{\frac{k_d}{m_d}} \qquad \textbf{Equation 5}$$

And damping coefficient of the tuned mass is given by:

$$c_d = 2\xi_d \omega_d m_d \qquad \textbf{Equation 6}$$

The governing equations of motion for primary mass and tuned mass are given by

$$\text{Primary mass } (1+\frac{m_d}{m})\ddot{u} + 2\xi\omega\dot{u} + \omega^2 u = \frac{p}{m} - \frac{m_d}{m}\ddot{u}_d \qquad \textbf{Equation 7}$$

$$\text{Tuned mass } \ddot{u}_d + 2\xi_d\omega_d\dot{u}_d + \omega_d^2 u_d = \ddot{u} \qquad \textbf{Equation 8}$$

Here, *p* refers to periodic excitation acting on the primary mass. For an optimal design of a tuned mass damper, the angular frequency of the tuned mass should approximate to that of the primary mass, i.e.

$$\omega_d = \omega \qquad \textbf{Equation 9}$$

The response with no damper system is given by:

$$\hat{u} = \frac{\hat{p}}{k}(\frac{1}{2\xi}) \qquad \textbf{Equation 10}$$

While the response with damper system is given by:

$$\hat{u} = \frac{\hat{p}}{k}\frac{m}{m_d}\sqrt{\frac{1}{1+(\frac{2\xi m}{m_d}+\frac{1}{2\xi_d})^2}}$$ **Equation 11**

There is a 90^o phase difference of the motion between the response of the tuned mass and that of primary mass. This phase difference produces damper inertia force that contributes energy dissipation to the system. Hence, the mass damper system limits the motion of the structure from a particular excitation subjected[7].

The multiple tuned mass dampers is a set of TMDs in multiple numbers arranged in paralleled manner[10].

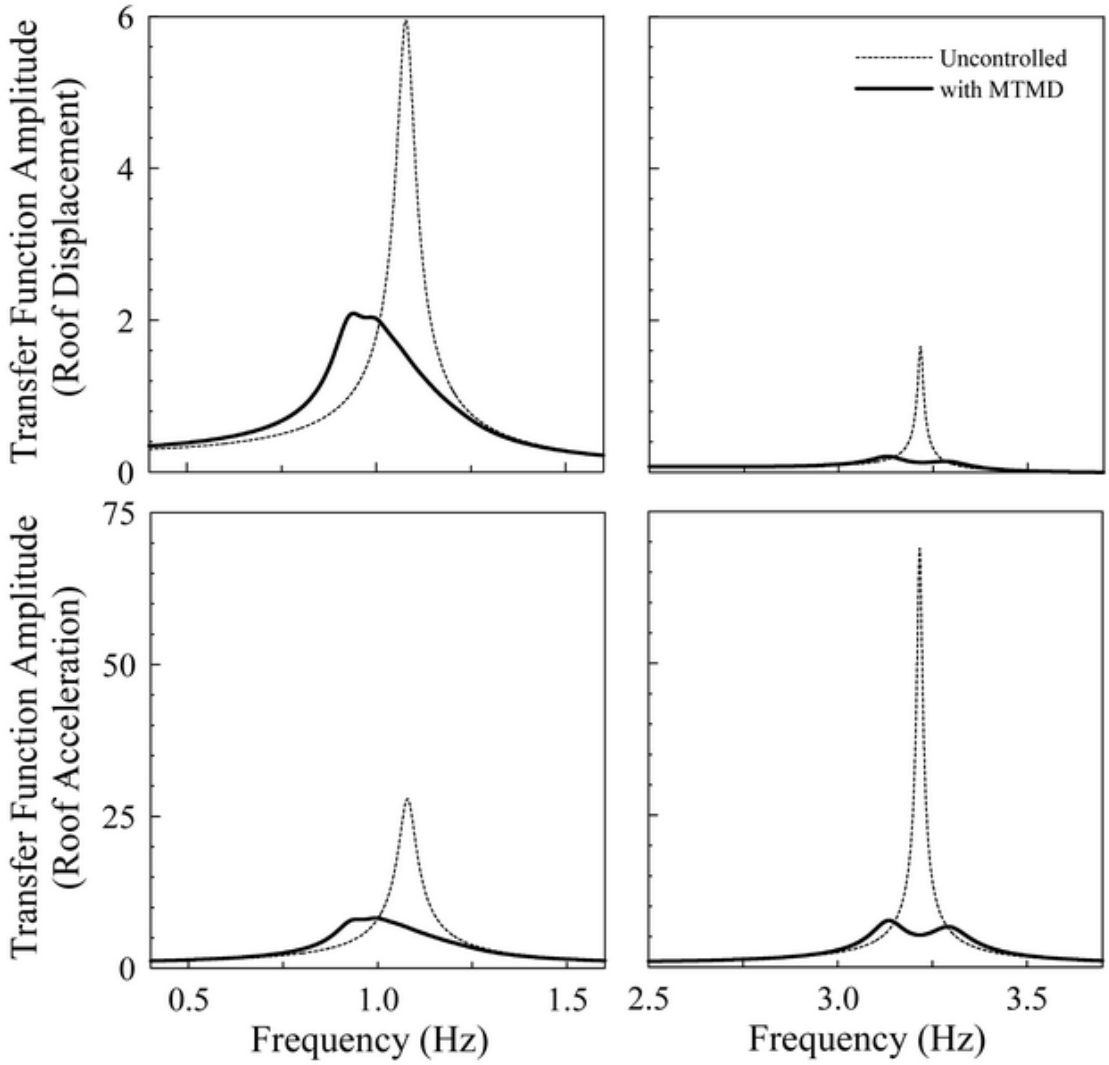

Figure 12. Typical transfer function in displacement and acceleration of experimental structure with and without MTMD, first mode of 1.08Hz and second mode of 3.42Hz.[10]

Figure 12 shows a typical transfer function of a structure subjected to an artificial white noise excitation. For the structure without MTMD, the structure has its resonance frequency with 1.08Hz of first mode and 3.42Hz of second mode. Here, first mode harmonic dominates displacement and second mode dominates acceleration. However, for the structure mounted MTMD, displacement and acceleration resonance peaks of the first mode and second mode are significantly suppressed[7, 10].

There are two types of common tuned mass dampers for improving the response of building structure against wind or seismic excitation, most likely on skyscrapers. Citicorp Centre (279m tall) in Manhattan, Canadian National Tower (553m tall) in Toronto, Chiba Port Tower (125m tall) in Chiba have installed the translational tuned mass dampers, the mass places on bearings that allow the mass to have movement laterally relative to the floor[11-14]. Taipei 101 Tower (508m tall) in Taipei, Crystal Tower (157m tall) in Osaka have adopted the pendulum tuned mass dampers in which the pendulum mass is attached to the floor through cables[15, 16].

2. Review of Previous Work

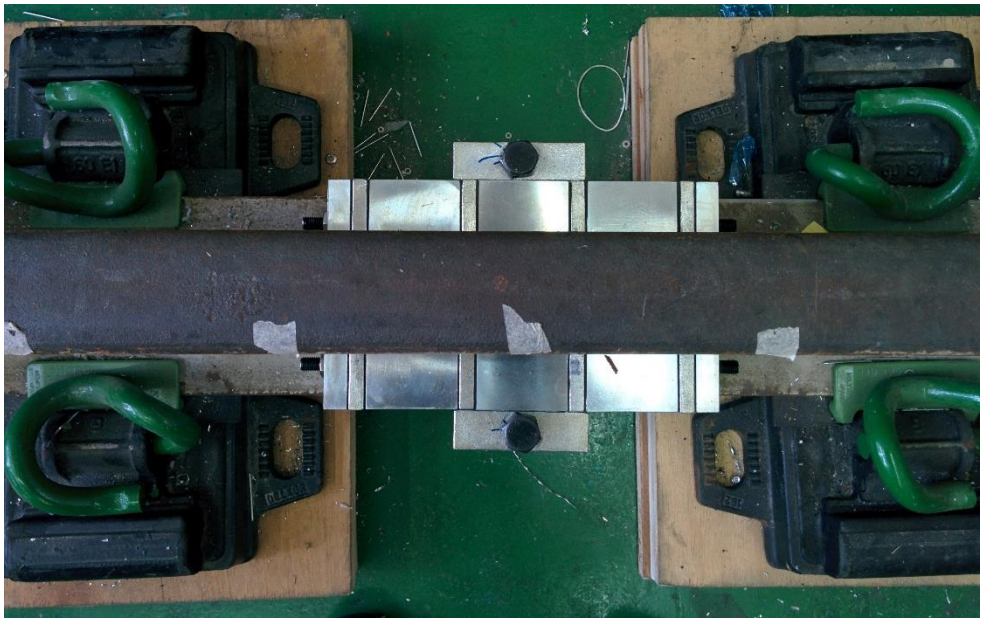

Figure 13. The top view of current design of TMD

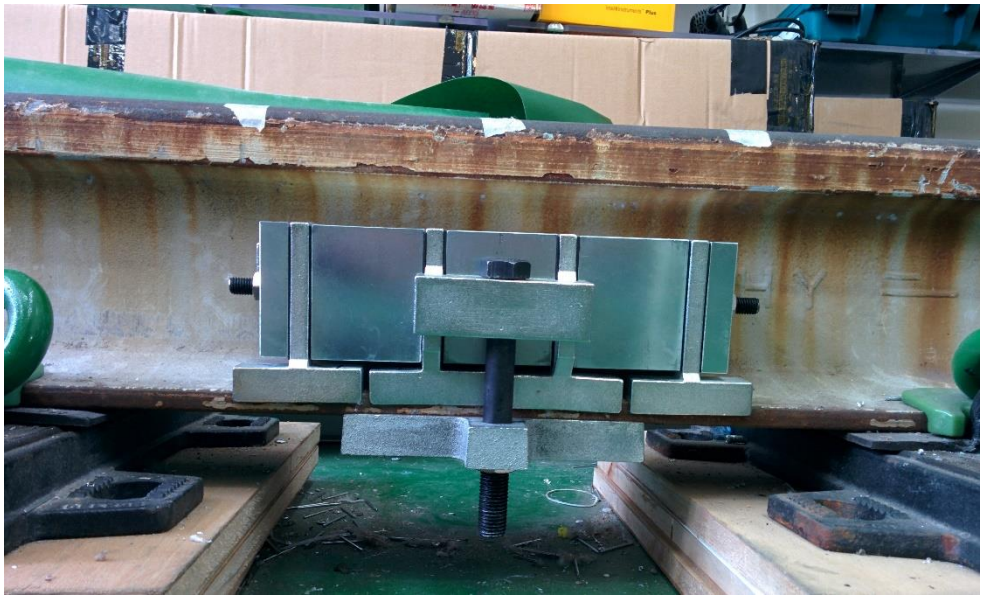

Figure 14. The side view of current design of TMD

In the previous chapter, the rolling noise, pinned-pinned resonance and principle of tuned mass damper module are briefly introduced. The development of the tuned mass damper

module in this study adopts multiple masses in a damper module considered as multiple tuned mass damper (MTMD). The schematic diagram of current design is shown in Figure 1 and the photos of the top view and side view are shown in Figure 13 and Figure 14, respectively. Here, the damper module contains two parts that are clamped on both sides of the railtrack. All six masses are deployed with three masses on each side so that the masses can oscillate along its shear direction of the resilient layers to complete a spring-mass system in both vertical and lateral directions. For a single unit of TMD shown Figure 15, mass and resilient layer are installed in series using screws and bolts. The mass has certain dynamic range which allows vibrations along various directions to absorb the energy from track.

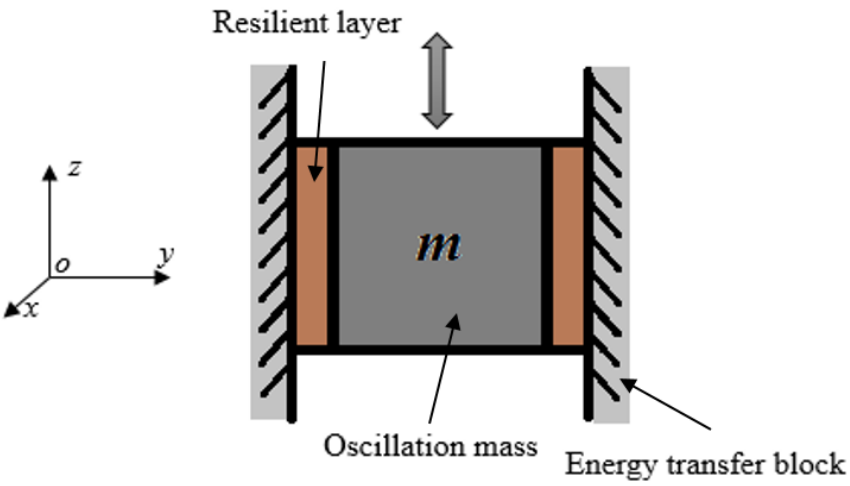

Figure 15. Schematic diagram of shear type spring-mass system

The resilient layers are placed on both sides of the oscillation mass that allow the mass to vibrate along *x*- and *z*- directions while minimizing the vibration along *y*- directions. The resilient layers have particular values of shear modulus to provide the mass a restoring force corresponding to the movement of the oscillation mass. The particular shear modulus can be determined through Equation 14, which is derived from Equation 12 and

Equation 13. The spring-mass system can be tuned to appropriate damping frequency for various purpose by introducing different shear modulus of the resilient layer.

Resonance frequency for two springs in parallel:

$$f = \frac{1}{2\pi}\sqrt{\frac{2k}{m}} \qquad \textbf{Equation 12}$$

Shear modulus of the resilient layer:

$$G = \frac{\tau}{\gamma} = \frac{Fb}{A\Delta x} \qquad \textbf{Equation 13}$$

where in, F is the applied force
τ is the shear stress
γ is the shear strain

Combined Equation 12 and Equation 13 the resonance frequency can be given:

$$f = \frac{1}{2\pi}\sqrt{\frac{2GA}{mb}} \qquad \textbf{Equation 14}$$

where in, G is the shear modulus of the resilient layer
A is the contact area
m is the oscillation mass
b is the thickness of resilient layer.

In Equation 14, the motion along lateral (x-direction) and vertical (z-direction) are independent to each other. Therefore, different resonance frequencies are possible to achieved by selecting a resilient layer with orthogonal shear moduli. Thus, a single oscillation mass element will be able to reduce two pinned-pinned resonance modes in orthogonal directions. Since the resonance frequency is proportional to the square-root of the shear modulus, with the fact that the frequency ratio between vertical and lateral pinned-pinned resonance modes is about 2, a ratio of 4 between the shear moduli of the two respective directions is required to have a TMD for application in reducing the noise for vertical and lateral directions.

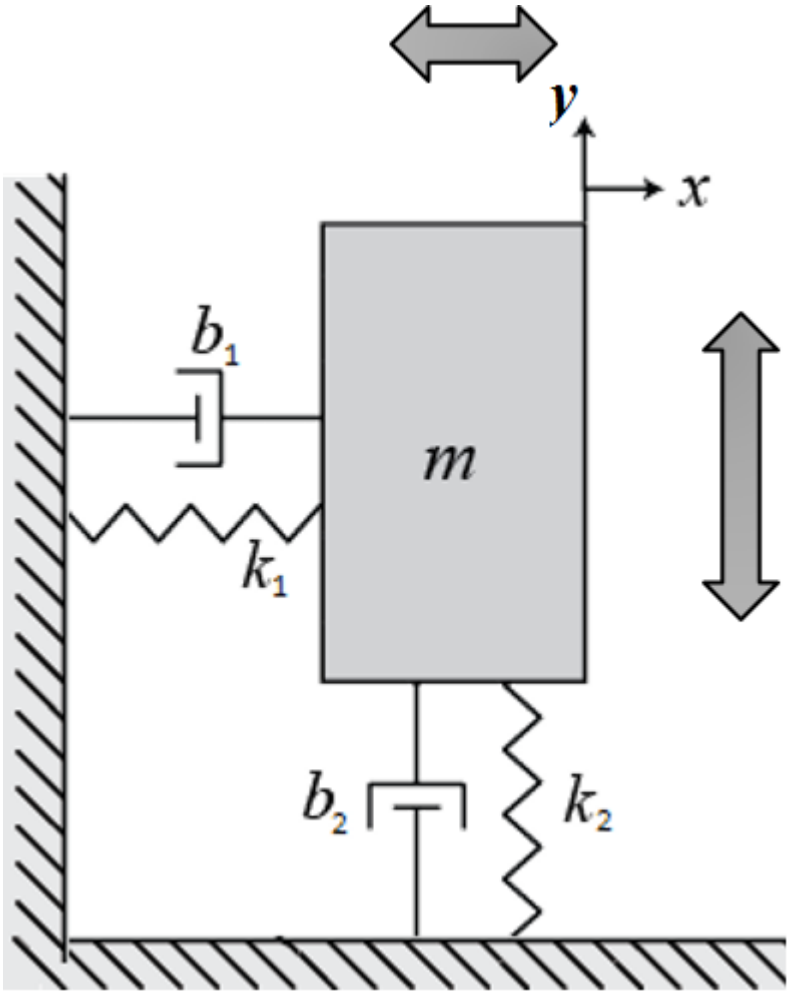

Figure 16. Illustration of the resilient layer demonstrating "spring-mass system" in lateral and vertical direction.

Figure 16 shows an illustration of the orthogonal resilient layer demonstrating "spring-mass system" in lateral (along *x*) and vertical (along *z*) direction. For an isotropic resilient layer, the mechanical properties along *x*- and *z*-directions are identical, k_1 and k_2 will be equal. However, for orthogonal resilient layer that has different shear moduli along *x*- and *z*-directions, k_1 and k_2 will be different. In the application of this study, in order to tune the mass damper system for higher frequency of vertical pinned-pinned resonance mode, k_2 is expected to have higher value than k_1, which means a higher shear modulus in *z*-direction than x-direction, i.e. orthogonal shear moduli for single resilient layer.

To produce an orthogonal resilient material to suppress two perpendicular directions of railtrack's pinned-pinned resonance modes, an orthogonal composite will be used to achieve a higher shear stiffness in particular direction by embedding aligned fibres into the resilient material in this study[17]. The fabrication and performance of this composite will be focused in this study.

3. Study of Computational Model

A computational model using finite element analysis (FEA) was developed through ANSYS to estimate and optimize the orthogonal shear moduli of composite. The purpose of developing computational model is mainly for studying the relations between fibre configuration and shear moduli in both vertical and lateral directions. The results of this study would provide a guidance for the preparation of orthogonal resilient layer.

Copper fibre was employed in our computational model. Copper fibre stripes. In this study, the optimal configuration for the fibres was examined. So that the composite can obtain the suitable shear moduli ratio in vertical and lateral directions. A series of AutoCAD drawings were created accordingly to import to the ANSYS to conduct FEA simulation.

3.1. Introduction to Finite Element Analysis (FEA)

The finite element analysis (FEA) is a mighty computational technique to determine approximate solutions for variety of real engineering problems that have general boundary conditions in complex domains. In numerous engineering disciplines, analytical solutions do not exist or difficult to be found. In the meantime, FEA has developed into a vital tool for physical phenomena in the design and modeling stage. The physical phenomena involved in the model usually associates in a continuum of matter, including gas, liquid or solid and involving several field variables. These field variables change from point to point, therefore processing an infinite number of solutions in the domains. Here, domain usually refers to a continuum with a known boundary[9, 18, 19].

The principle of FEA bases on the decomposition of domain into a finite number of subdomains, also called elements. Hence, the systematic approximate solution is determined by applying the variational or weighted residual methods. FEA simplifies the problem into a finite number of unknowns by partitioning the domains into elements and expressing the unknown field variables as the assumed approximating functions in each element. These functions are called interpolation functions. They are defined into the field variables' value at specific points, which are called nodes. These nodes are usually placed along the element's boundaries, thus the nodes connect adjacent elements. FEA is considered as a valuable and practical analysis tool for finding the solution of boundary, initial and eigenvalue problems in numerous engineering disciplines due to FEA's ability to discretize the irregular domains with finite elements. There are seven major steps that FEA are required[9, 18],

1. Discretization of the domain into a finite number of elements.
2. Selection of interpolation functions.
3. Development of the element matrix for the element.
4. Assembly of the element matrices for each element to obtain the global matrix for the entire domain.
5. Imposition of the boundary conditions.
6. Solution of equations.
7. Additional computations (if desired).

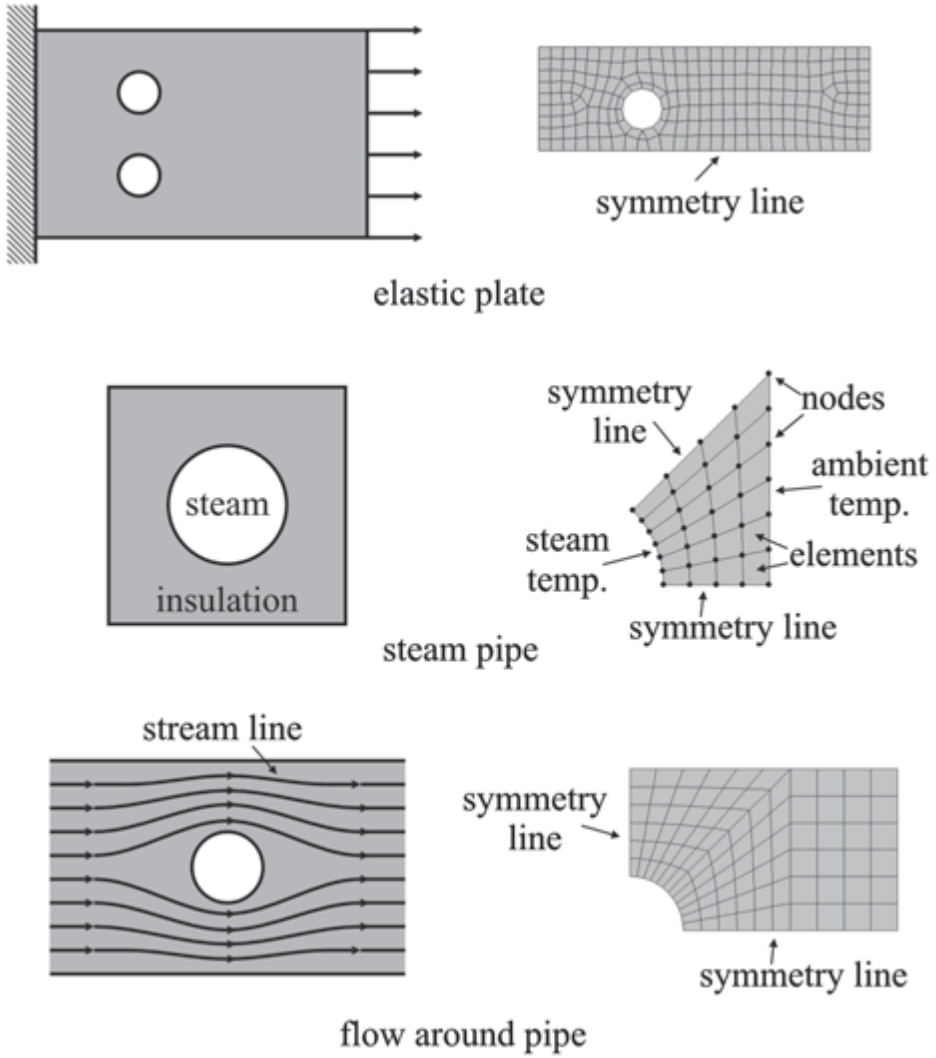

Figure 17. FEA representation of practical engineering problems[9]

Figure 17 shows the FEA discretizations from domain into elements that using common engineering problems. For example, elastic plate, steam pipe in thermal dynamic and flow dynamic around object.

3.1.1. Nodes

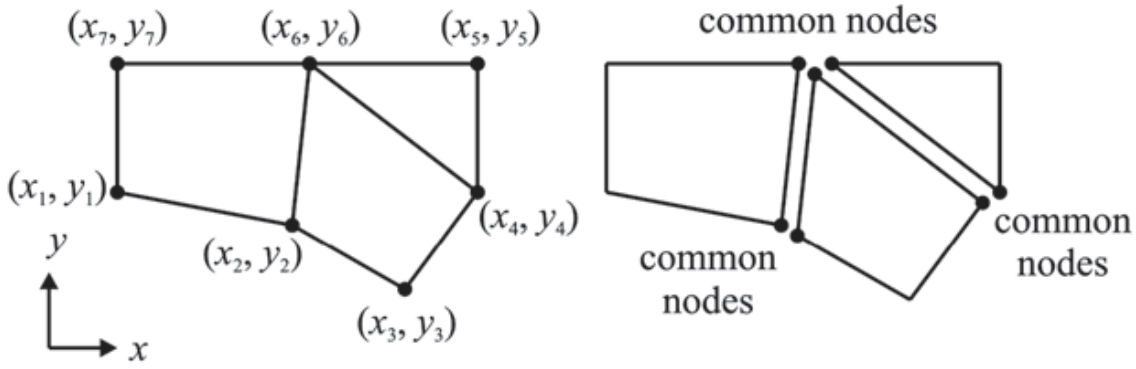

Figure 18. Decomposition of a domain into elements[9]

Figure 18 shows a practical engineering problem transformed into a mathematical representation through discretizing the domain of interest into elements. All elements are connected to each other by their "common" nodes. A node has corresponding coordinate location in space where degrees of freedom and actions of the physical problem exist. The unknowns of node in the matrix system of equations represent one or more of the primary field variables. Variables of node assigned to an element are called the degrees of freedom of the element. The common nodes in Figure 18 provide continuity for the degree of freedom (DOF). DOF of a node are determined by the physical nature of the problem and the element type. The DOF and corresponding "force" used in FEA for different physical problems can be referred to Table 1[9, 18].

Table 1. Degrees of freedom and force vectors in FEA for different engineering disciplines[9]

Discipline	DOF	Force vector
Structure / solids	Displacement	Mechanical forces
Heat condition	Temperature	Heat flux
Acoustic fluid	Displacement potential	Particle velocity
Potential flow	Pressure	Particle velocity
General flows	Velocity	Fluxes

Electrostatics	Electric potential	Charge density
Magnetostatics	Magnetic potential	Magnetic intensity

3.1.2. Elements

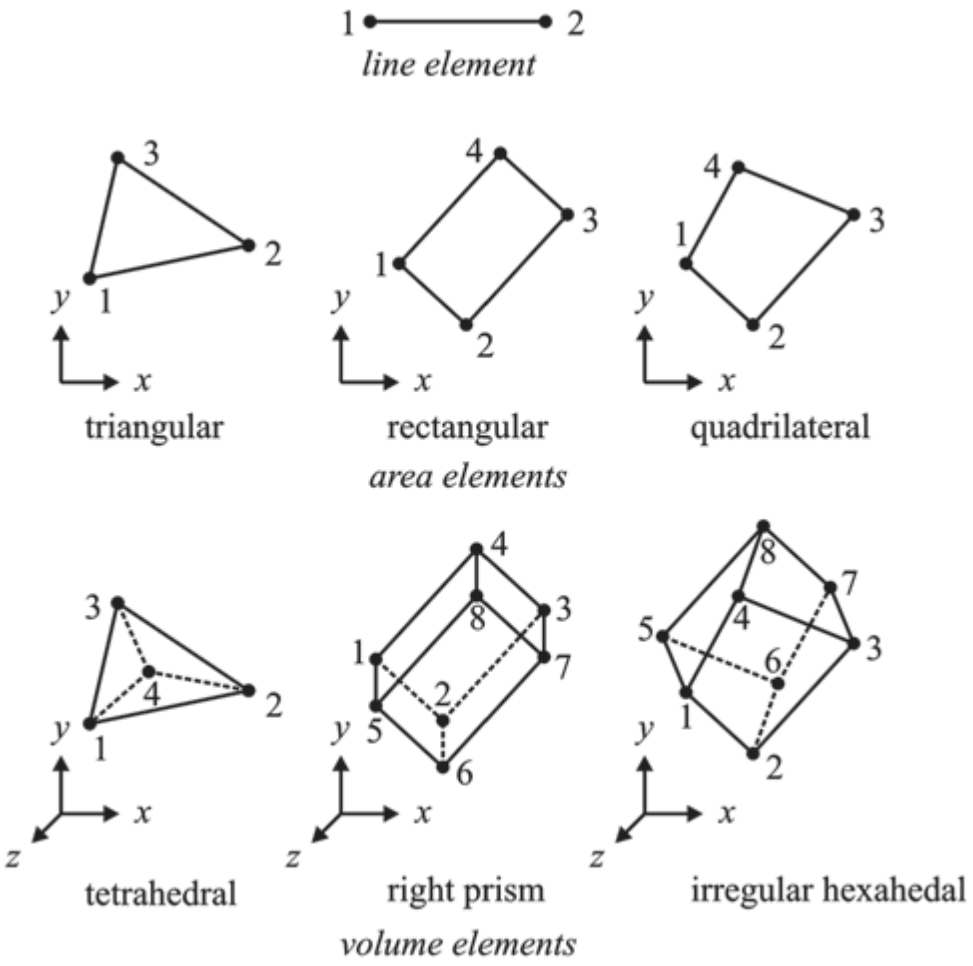

Figure 19. Description of line, area, and volume elements with node numbers at the element level[9]

The domain of interest can be discretized by employing line, area, or volume elements based on the geometry and the physical nature of the problem. Some FEA common element examples are listed in Figure 19. Each element with noted by an element number, is defined by a specific order with node numbers. The specific order is based on the node numbering at the element level. Depending on the discipline of the engineering problems,

each nodal variable will be substituted into corresponding matrix system of equations to determine unknown variables that will solve the engineering problems[9, 18].

3.2. Material's Physical Parameters for FEA

In the computation model, a branch of materials' physical parameters is required to simulate the effect on the system with loading. ANSYS consists a database that contains numerous parameters for common engineering materials. These parameters include mechanical, thermal, electrical and magnetic properties. In this study, mechanical properties are considerably more important.

There are only two materials adapted in this study, they are copper as fibres and neoprene rubber as matrix of the composite. Copper is a typical linear elastic material, the properties and behaviours within elastic deformation are able to be described through Young's Modulus, Bulk Modulus, Shear Modulus and Poisson Ratio[20]. The parameters listed in Table 2 are extracted from ANSYS database and have been used in our FEA study.

Table 2. Copper's mechanical properties for FEA

Young's Modulus	110.0 GPa
Poisson's Ratio	0.34
Bulk Modulus	114.6 GPa
Shear Modulus	41.05 GPa
Tensile Yield Strength	280.0 MPa
Compressive Yield Strength	280.0 MPa
Tensile Ultimate Strength	430.0 MPa

However, neoprene rubber is a hyperelastic material, whose elastic behaviour is not linear. Therefore, the stress-strain relation cannot simply be described in various moduli i.e. it is

difficult to assign a single modulus to be represented as the properties of linear materials. The stress-strain relations of hyperelastic materials are described through corresponding stress-strain curves, which usually obtained by experiments[21]. The stress-strain curves listed in Figure 20 are extracted from ANSYS database and have been used for our FEA study.

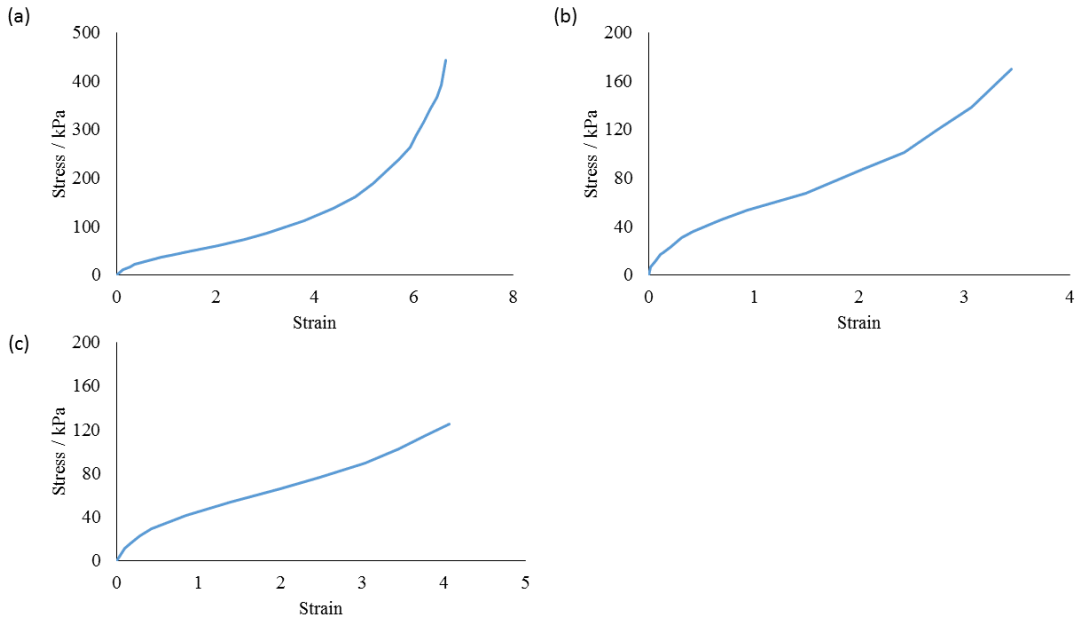

Figure 20. The stress-strain curves of neoprene rubber for FEA, (a) under uniaxial tensile condition, (b) under biaxial tensile condition and (c) under shear condition.

The ANSYS applies Newton-Raphson Method to solve nonlinear problems. The loading is subdivided into a series of load increments. The load increments can be applied over several load steps. The top level consists of the load steps that has been defined clearly over a "time" span. Within the load steps, loads are assumed to vary linearly. Within each load step, the programme performs several solutions to apply the load gradually. At each sub-step, the programme will run a number of equilibrium iterations to obtain a converged solution[9].

3.3. Composite Dimension and Fibre Configuration

In the computational model, the dimensions of composite, the appearance size of the composite, were kept constant as the same dimensions of mold in our measurements, which are 72mm in length, 54mm in width and 3mm in height. A series of AutoCAD drawings is created in various conditions to simulate the effect on the number of embedded fibres stripes to the shear moduli in vertical and lateral directions. Figure 21 shows a 3D drawing of the composite in top view, side view and isometric view in wireframe style. The fibres were erected inside the matrix and aligned in parallel manner to the 72mm side, they are 0.1mm in thickness, 2mm in height and 72mm in length, which is end-to-end in the matrix. These fibres are also set distributed evenly in the matrix.

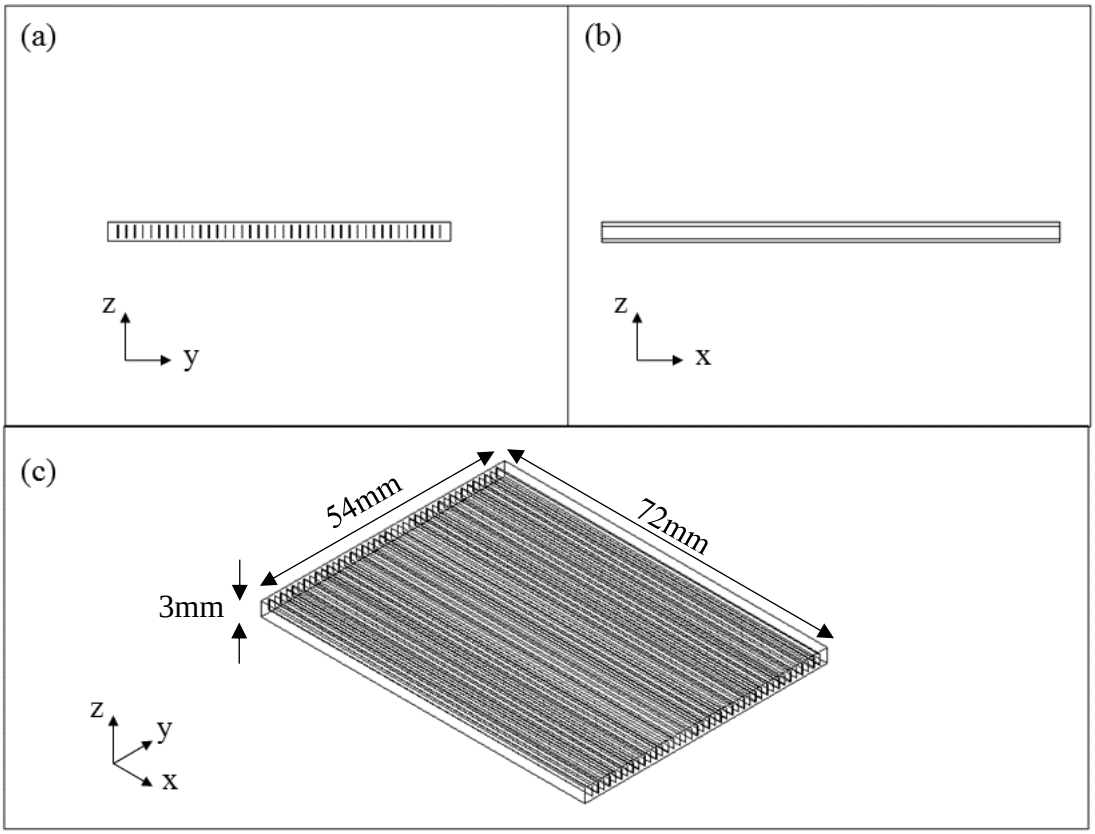

Figure 21. (a) Top view, (b) side view and (c) isometric view of composite's CAD drawings.

3.4. FEA Solver and Condition

A static structural solver in ANSYS was adopted in this study. The effects of steady loading acting on a structure can be calculated through a static structural solver without considering the effects inertia and damping. Those effects caused by loadings include the displacement, stresses, strains, and forces in structures. The static structural solver is able to handle linear and nonlinear analysis, which consists of large deformations and hyperelastic elements that are essential in this study [9].

There are three major steps in static analysis' procedure: first, building the model; second, setting boundary conditions, applying loads and obtaining the solution; third, reviewing the results.

3.4.1. Building the Model

The CAD drawings were exported to ANSYS. The matrix part was set as neoprene rubber and the fibres was set as copper stripe. All contact surfaces were set bonded to illustrate a prefect adhesion between the matrix and the fibres in composite.

Table 3. Meshing conditions of FEA

Sizing	
Relevance Centre	Coarse
Smoothing	Medium
Transition	Fast
Inflation	
Inflation Option	Smooth Transition

To obtain a more accurate result, fine mesh, high smoothing, slow transition in sizing are much more preferred. However, the education license of ANSYS limits the number of

element in the computational model that we could select. In this study, the optimal option was adopted. In the meshing section, all the models were set as Table 3 and the meshing is done automatically through ANSYS.

Since the model involves hyperelastic materials, it is necessary to allow large deformations in the computation.

3.4.2. Applying Loads and Obtaining the Solution

The model is intended to figure out the shear moduli in the lateral and vertical directions, through calculating the shear deformation under applying certain shear loading.

The fixation of the model was appointed on the whole negative-z surface, the 10N of directional force applied on the whole positive-z surface. For lateral shear deformation, a 10N force towards +*y*-direction was set to act on the whole surface. For vertical shear deformation, a 10N force towards +*x*-direction was set to act on the whole surface. The illustrations are shown in Figure 22.

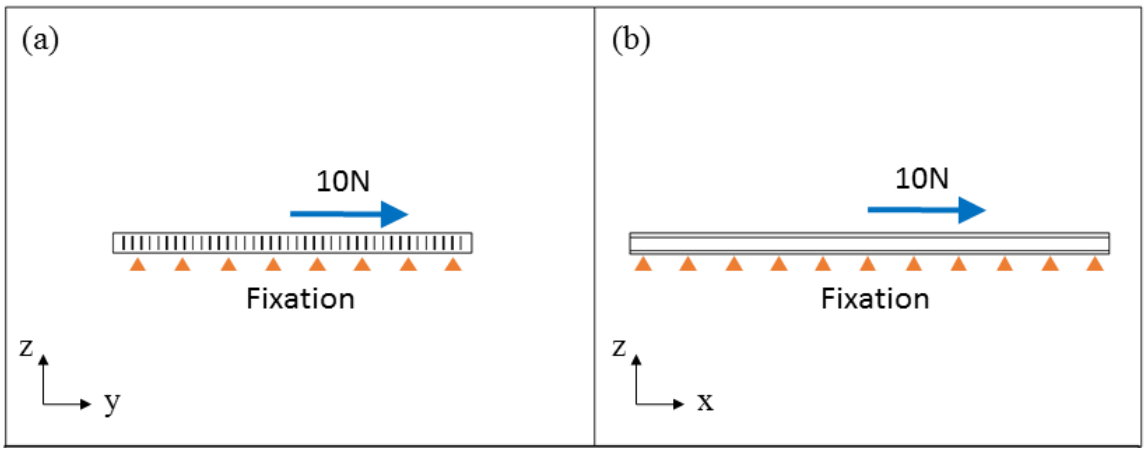

Figure 22. Illustrations of applying loads for FEA (a) *y*,*z*-plane view and (b) *x*,*z*-plane view

The deformation on the surface was recorded and then the corresponding shear modulus was determined through Equation 13 accordingly.

3.5. FEA Results and Analysis

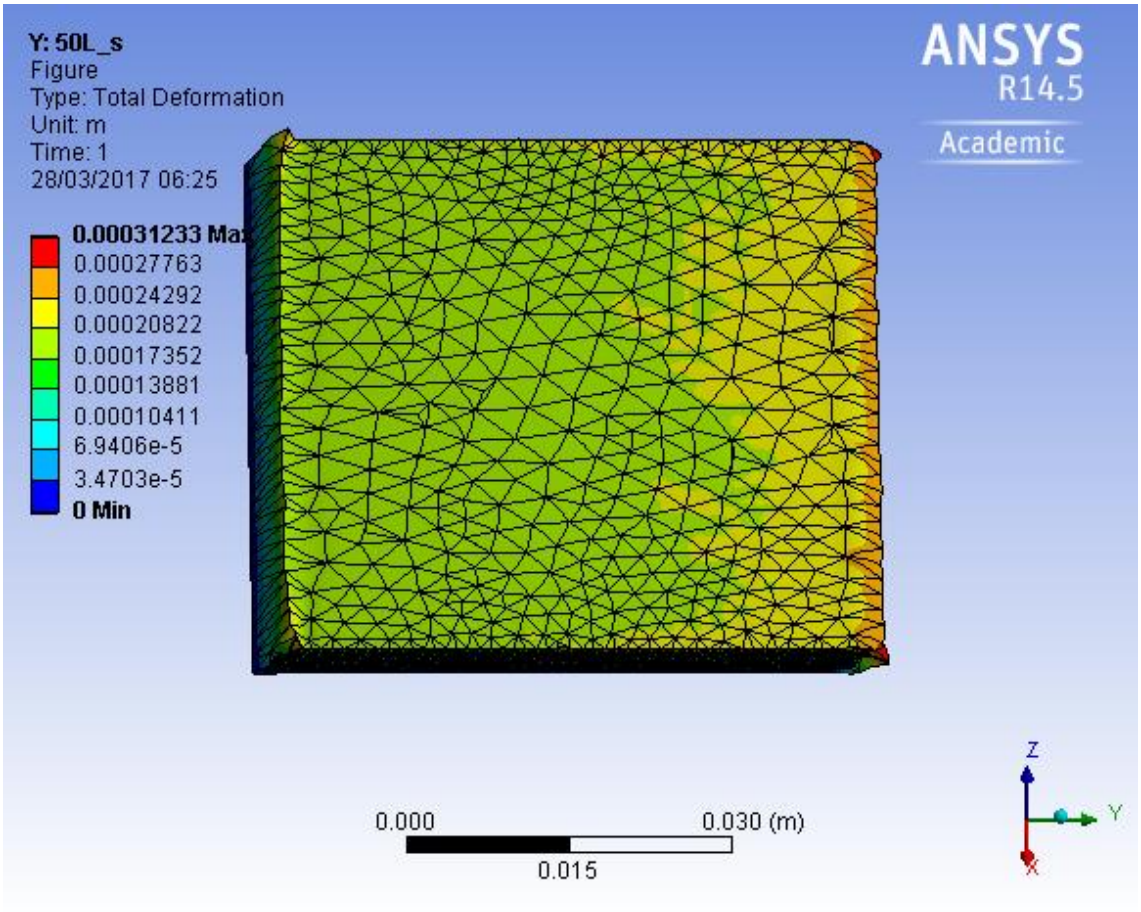

Figure 23. The FEA deformation of composite under lateral shear loading (50 stripes embedded)

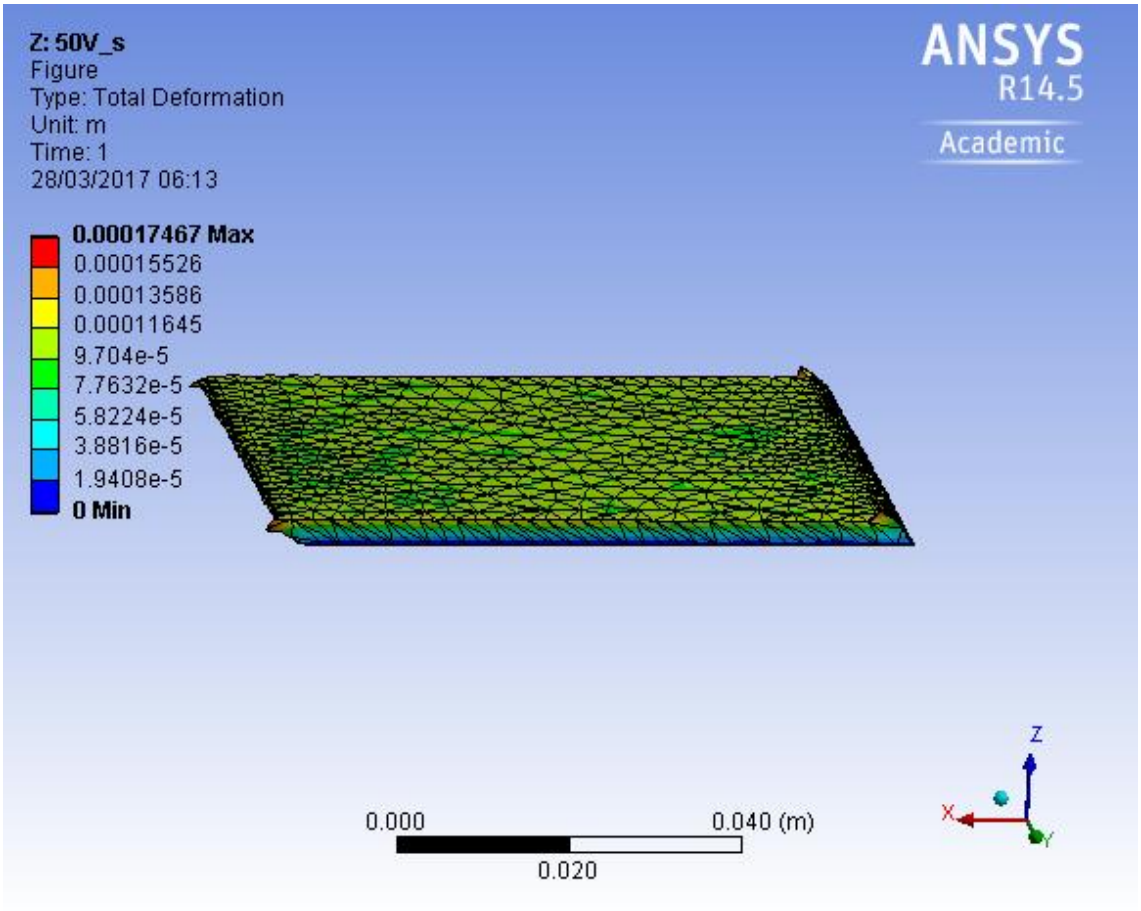

Figure 24. The FEA deformation of composite under vertical shear loading (50 stripes embedded)

In Figure 23 and Figure 24, the pictures show the total deformation of the composite under lateral and vertical shear loading.

To investigate the effects of number of copper stripe on shear moduli ratio. In our FEA, there were eleven configurations in total, from zero copper stripe embedded into the silicone matrix (homogeneous material) to that of 100 copper stripes. The maximum shear modulus ratio is at 50 stripes embedded composite, which has shear moduli ratio of 2.03. In Figure 25, the shear moduli ratio increases rapidly from number of stripe of zero and reaches the maximum value of ~2.03 at 50, then the ratio starts to decay gradually and seems to become constant at large stripe number. However, a bulge is observed at the number of stripes equals to 20.

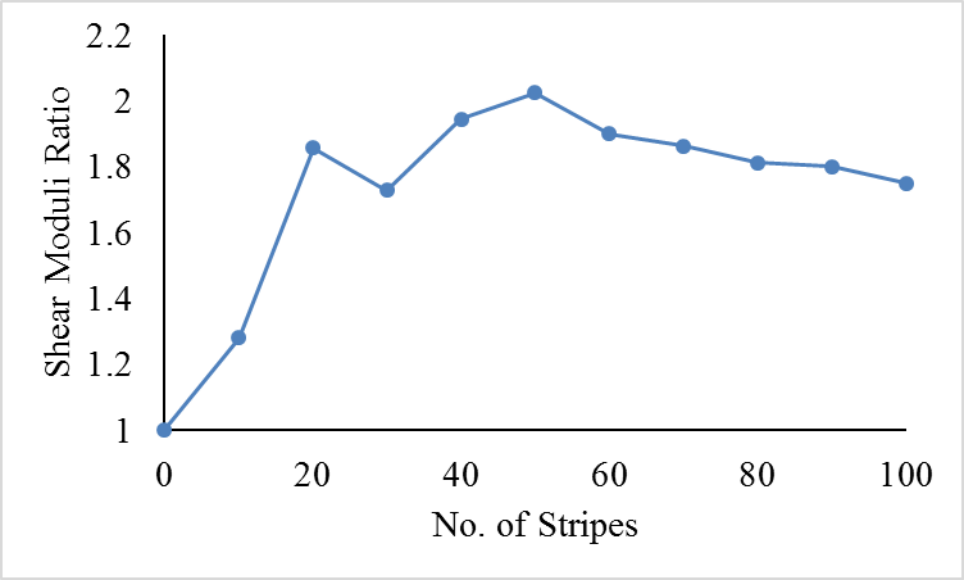

Figure 25. The graph of shear moduli ratio against Number of stripes extracted from FEA

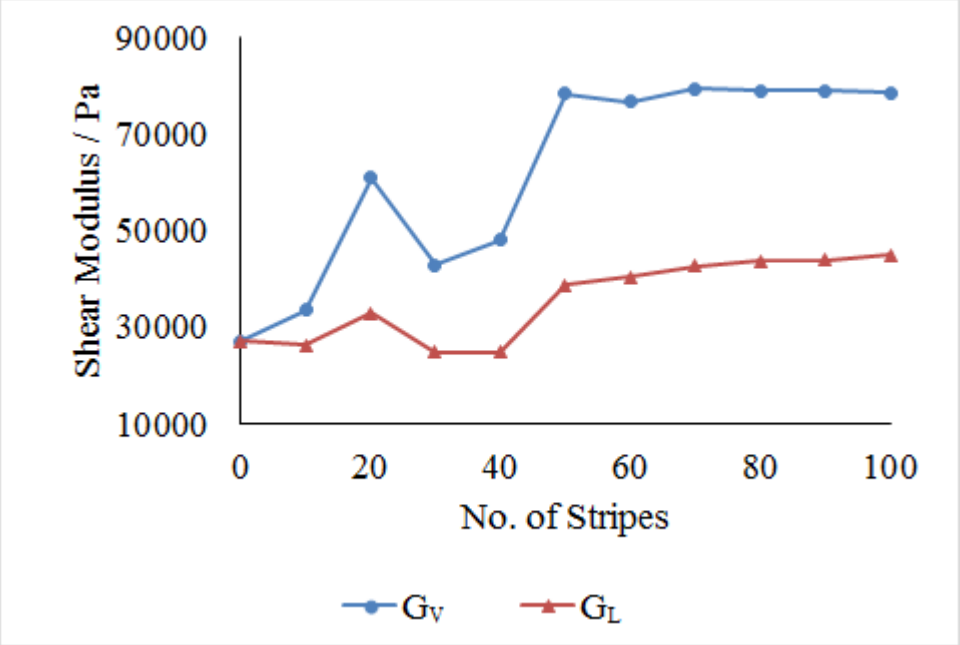

Figure 26. The graph of shear modulus against Number of stripes extracted from FEA

Refer to the Figure 26, except the data of 20 stripes embedded, both lateral and vertical shear moduli increase gradually till 50 stripes embedded. Vertical shear moduli remain and lateral shear moduli gradually increase which explains the decay in the later part of Figure 25.

Figure 26 shows both vertical and lateral shear moduli have similar trend as the number of stripes increase but the vertical shear moduli increase greater than the lateral shear moduli, hence, the ratio increase as the number of stripes increase.

4. Study of Orthogonal Materials

Due to the railtrack cross-section profile, the pinned-pinned resonance modes of the railtrack in lateral and vertical directions are in the frequency ratio of around 1:2. Based on the principle of tuned mass damper system, the resonance frequency is proportional to the square root of the shear modulus of the resilient layer. Therefore, a ratio of 4 between the shear moduli of the two respective directions is required in order to control the lateral and vertical pin-pin resonance modes with a frequency ratio of about 2. For such situation, two sets of resilient layers are prepared to demonstrate the hypothesis of the multidirectional tuned mass damper module. In this study, two types of aligned fibres, glass fibre and copper stripes, have been embedded into the silicone matrix to form a composite resilient layer with orthogonal shear moduli. All the samples were measured by a tensile tester Instron8800 with a holder that allows samples' shear properties to be measured. In this study, the measurements were based on ISO-1872. In fact, a neoprene rubber is preferable to be the matrix material in the study, due to the fact that neoprene is used as the TMD in real situation. WAL is adopting neoprene rubber as the material of isotropic resilient layer in their current TMD design. However, the fabrication of the neoprene rubber requires a hydraulic heat press machine for the curing and the moulding process. Therefore, silicone due to its easily fabrication process, was selected as the matrix in order to verify the concept of orthogonal resilient layer.

Vibration tests were conducted to figure out the resonance frequency of the tuned mass damper module, which provided a direct information for the performance of the orthogonal materials.

4.1. Preparation of Glass Fibre Reinforced Composite

In order to produce an orthogonal material that has higher shear moduli in specific direction, glass fibre was first embedded into the silicone matrix. The glass fibre was embedded into the silicone in a sandwich manner, i.e. alternative silicone and glass fibre layers. Each silicone layer had a thickness of 0.5mm, and covered by an aligned and well-dispensed glass fiber layer. In our study, the glass fibre reinforced composite consisted of five layers of silicone and four layers of glass fibre.

A Teflon mould is made with a slot for casting the composite, according to the dimension of composite, which was kept at 72mm in length, 54mm in width and 5mm in height.

Figure 27. Teflon mould for casting composite

Based on our measurement, the base matrix was made of a RTV-2 silicone rubber, with Young modulus of 311kPa and shear modulus of 107kPa. The silicone mixed with curing

agent in ratio of 1:100, was poured into a Teflon mould. For each layer with 0.5mm thickness, the silicone weighted 2.40g, which is 12.00g for totally five layers. Then, the silicone was put into a vacuum chamber to remove gas bubbles, as there were gas bubbles created in the silicone while mixing the silicone with the reagent. The curing process lasted for three hours in an oven at 75°C. Figure 28 shows the schematic flowchart for the fabrication process.

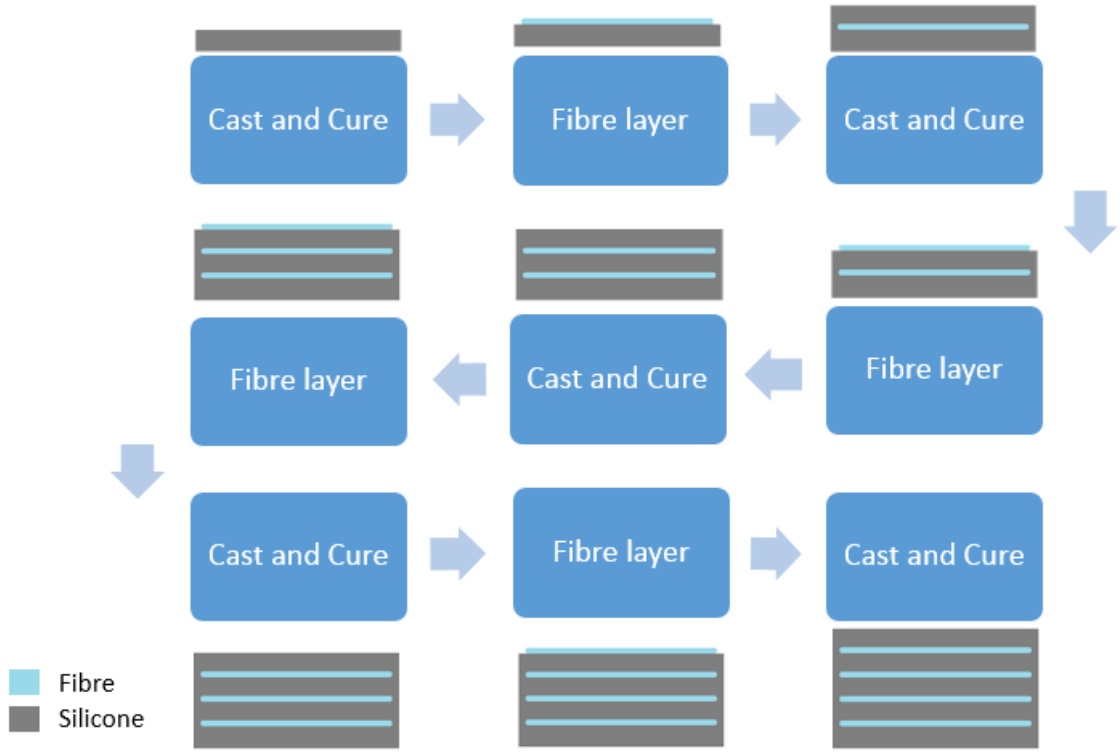

Figure 28. Flowchart of fabrication process of glass fibre reinforced composite

E-glass fibre with diameter of 20μm and Young modulus of 70GPa was selected as the type of fibre embedded in the composite due to its high acid resistance and ease to acquire. Indeed, it is a common commercial glass fibre with low cost. The glass fibres were chopped into 72mm in length. The glass fibres were stored in a bunch holding together with glue when purchased. Thus, before forming the new layer of silicone on top, glass

fibres needed to be cleaned using ethanol. While the glass fibres were still soaking in ethanol, they were placed and distributed in the mould.

The dimension of the composites was 72mm in length and 54mm in width (same as the Teflon mould), and the height was kept at 3mm.

Table 4. Parameters for matrix and fibre of composite

	Matrix	Fibre
Material	RTV-2 Silicone Rubber	E-glass fibre
Young Modulus	311 kPa*	70 GPa#
Shear Modulus	107 kPa*	--
Diameter	--	20 μm
Mass	12.0g	0.7g - 4.9g
Mass ratio	81.1%	0% - 18.9%
Cross-section ratio	88.4%	0% - 11.6%

* Measured value

Reference [17]

However, when the fibre was too dense in the layer, the upper silicone layer cannot attach to the lower layer well and this made the fibre layer totally separated from both silicone layers. The photo of composite with mass ratio of 18.9% is shown in Figure 29. In our measurements, we noticed that the detachment started at glass fibre weight of 4.9g, This means that the limitation of the amount of embedded fibres through this fabrication method is at mass ratio of 18.9%.

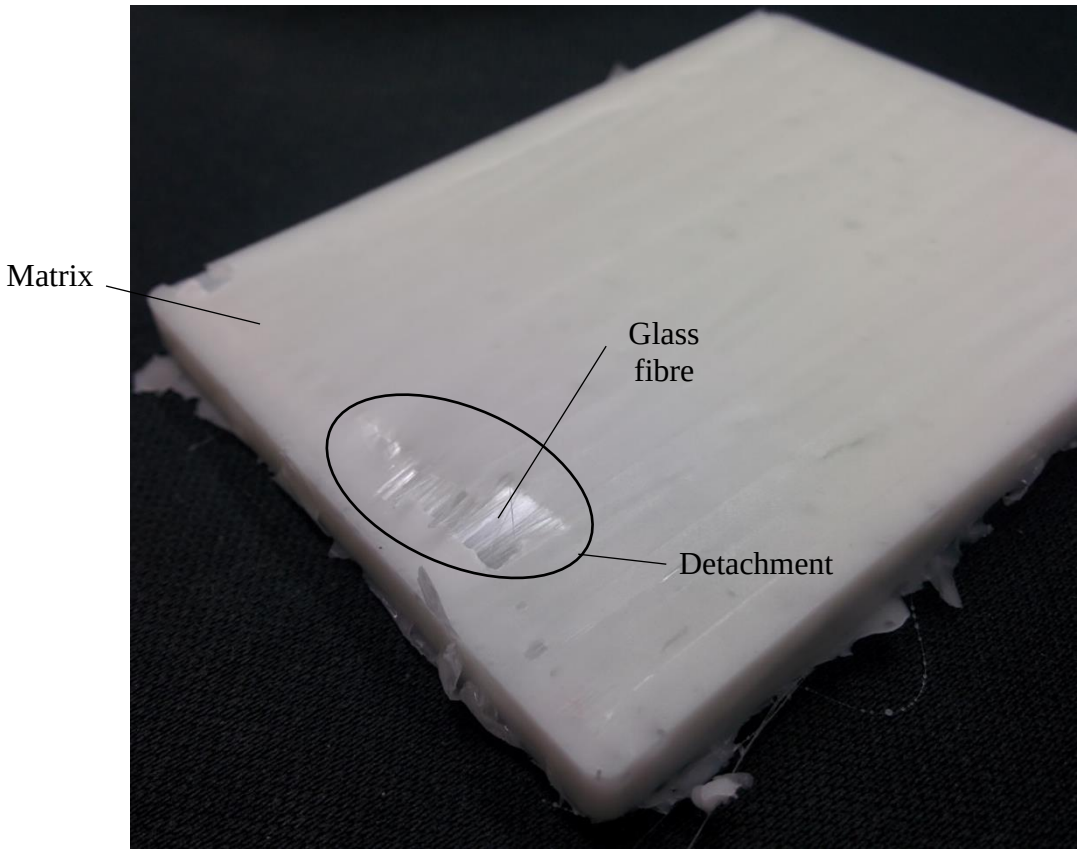

Figure 29. Detachment (marked in circle) between glass fibre and silicone matrix. The mass ratio of the composite is 18.9%

4.2. Preparation of Copper Stripe Reinforced Composite

Instead of embedding glass fibres, copper stripes were also embedded in the composite. The copper stripes were embedded in the silicone matrix vertically, which is similar to the setup of computational model. However, there were two differences here: first, the copper stripes had the thickness of 0.15mm instead of 0.1mm in FEA; second, beside using silicone as composite matrix, neoprene rubber was also employed in this study, to investigate the effect of embedded material on the properties of the composite. Indeed, neoprene rubber is more appropriate materials for the application considering its mechanical properties. But the fabrication of neoprene rubber involves a hydraulic heat

press machine to mould and cure the neoprene rubber. The fabrication process was performed in a factory located in Dongguan, China.

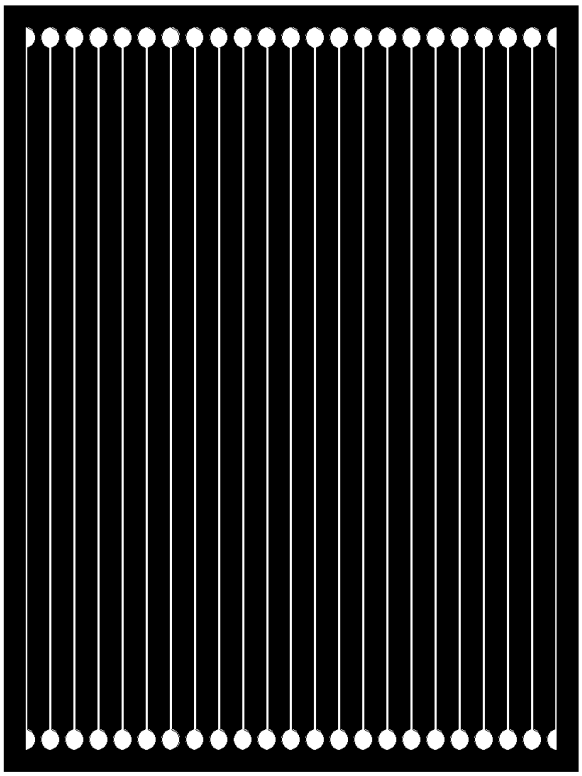

Figure 30. PCM pattern for the copper frame

In order to fixed the copper stripes in place inside the matrix, a copper frame was employed to erect the stripes. The copper frame designed in this study was shown Figure 30. In the design, a narrow joint was employed to hold the stripes and at the same time the joint can twist the stripes to be perpendicular to the frame. For different numbers of copper stripes, we could use the same design but of different density of copper stripes. The copper frames were fabricated through photo chemical milling (PCM). PCM can selectively etch certain part of a copper sheet to make a desirable pattern[22]. Figure 30 shows the design of the PCM pattern of the copper frame, which has 22 copper stripes per copper frame. Hence, the number of copper stripes embedded into the matrix will be the multiple of 22. The copper frame was flat after the PCM, it requires to twist the copper

stripes from flat to perpendicular to the frame, which the twisted frame is showed in Figure 31.

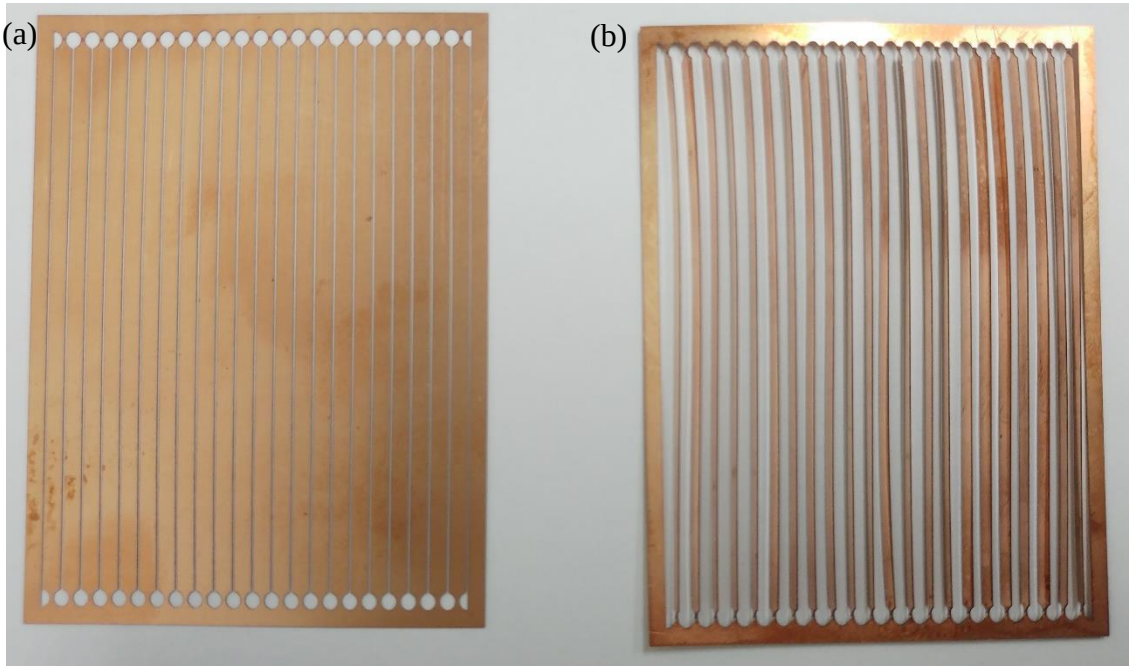

Figure 31. The copper frame (a) before twisting the stripes and (b) ready to be embedded.

In the fabrication section, the base matrix was made of RTV-2 silicone rubber, with Young modulus of 311kPa and shear modulus of 107kPa, similar to that of the matrix used in glass fibre reinforced composite. The silicone mixed with curing agent in ratio of 1:100, was poured into a Teflon mould. The silicone base has weight of 14.0g in total. Then, the copper frame was placed into the silicone. Next, the silicone and copper frame was put into a vacuum chamber to remove gas bubbles, since there were gas bubbles created in the silicone while mixing the silicone with the reagent. The curing process lasted for three hours in an oven at 75^{o}C. The copper stripe reinforced composites had the same dimension as the glass fibre type, which was 72mm in length, 54mm in width and 3mm in height.

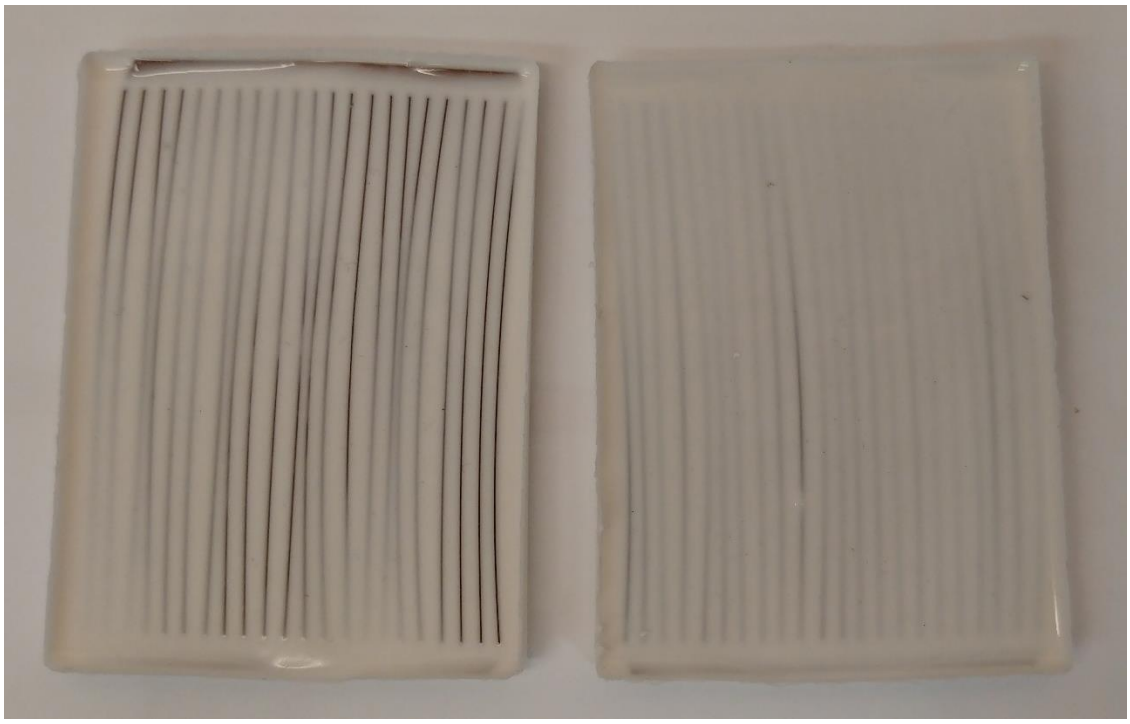

Figure 32. The photos of copper stripe reinforced composite without surface finishing

Figure 32 shows the photos of copper stripe reinforced composite without surface finishing. The copper frame totally merged into the silicone matrix. However, the surface of copper stripes was rather smooth, thus bad adhesion between silicone and copper stripes were observed, this slight detachment is shown in Figure 33. Therefore, a rough polishing on the copper frame surface before twisting the stripes was employed in order to improve the adhesion between the stripes and matrix.

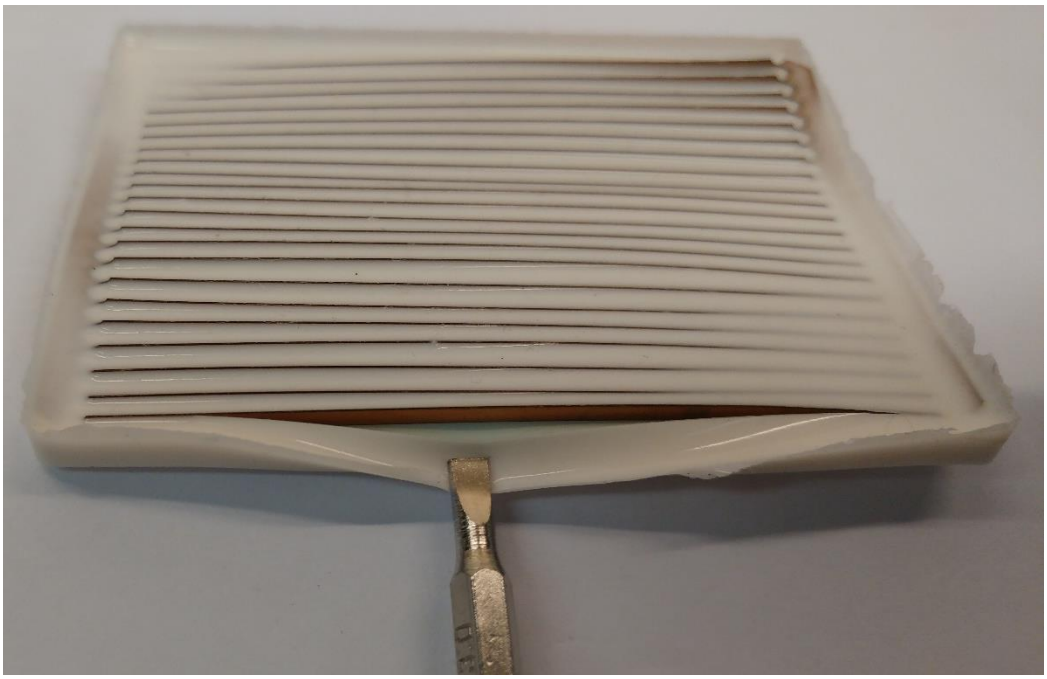

Figure 33. Detachment between copper stripes and silicone matrix (side view)

4.3. Mechanical Properties of resilient layer

The fibre reinforced composite's measurement details of shear moduli along lateral and vertical directions, the setup, measurement condition and results are introduced in this section.

4.3.1. Measurement Setup

The shear moduli measurement of the samples was based on ISO-1827:2011, which is an international standard for determining the shear modulus of rubber, vulcanized or thermoplastic and adhesion strength to rigid plates through quadruple shear method. Quadruple shear method requires a sample holder, shown in Figure 34, to allow the shear properties of the samples to be measured by a tensile tester. In Figure 34, four identical samples are bonded on their two opposite faces to the coupling faces of four rigid plates to obtain a symmetrical double-sandwich arrangement. The rigid plates should have enough thickness to withstand bending during the measurement. The rigid plates

employed in the measurements were 6061 aluminium alloy with thickness of 6.35mm (0.25in), consider that Silicone's Young modulus of 311kPa and that of 6061 aluminium alloy is 68.9GPa[23], it is noticed that 6061 aluminium alloy is capable to withstand the bending in the test. When the samples and sample holder were fixed in place, tensile tester started applying a traction force that provided constant travelling speed of the jaws at a rate of 5mm/min until a maximum shear strain of 0.3 was reached, and the force-deformation curve was recorded accordingly[24]. Instron 8872 testing system with actuator and load cell capable for 25kN loading was employed for the tests.

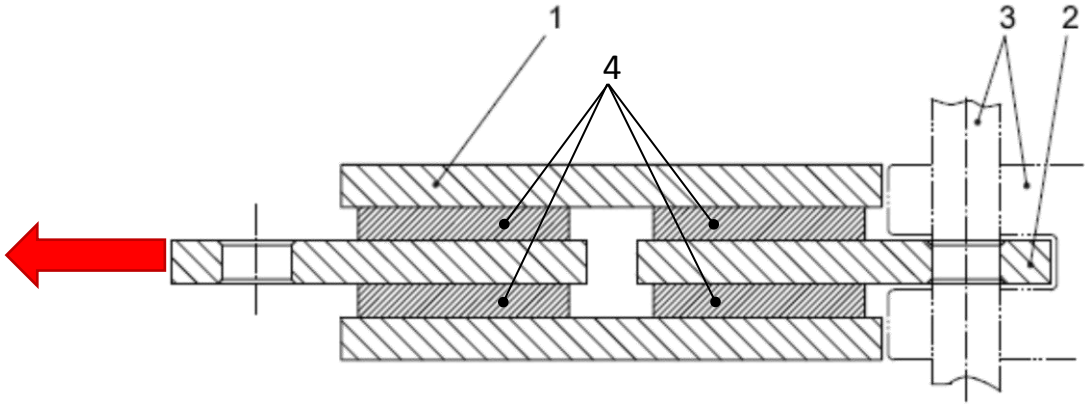

Figure 34. Sample holder for the shear modulus measurement, (1) – two external plates, (2) – two internal plates and (3) fixture for tensile loading, (4) samples [24]

In our measurements, there were two amendments from ISO1827. First, ISO1827 suggests that the sample should be 4 mm ± 1 mm thick, 20 mm ± 5 mm wide and 25 mm ± 5 mm long. In our test, the sample dimension was 3mm thick, 54mm wide and 72mm long because this dimension set will be the same as adopted in the vibration tests i.e. same dimension as the dimension of damper mass in the vibration tests. Second, instead of glue fixation between rigid plates and samples that suggested in ISO1827, two C-clamps were deployed during the measurements to provide fixation to prevent damage to the samples during ungluing, shown Figure 35[24].

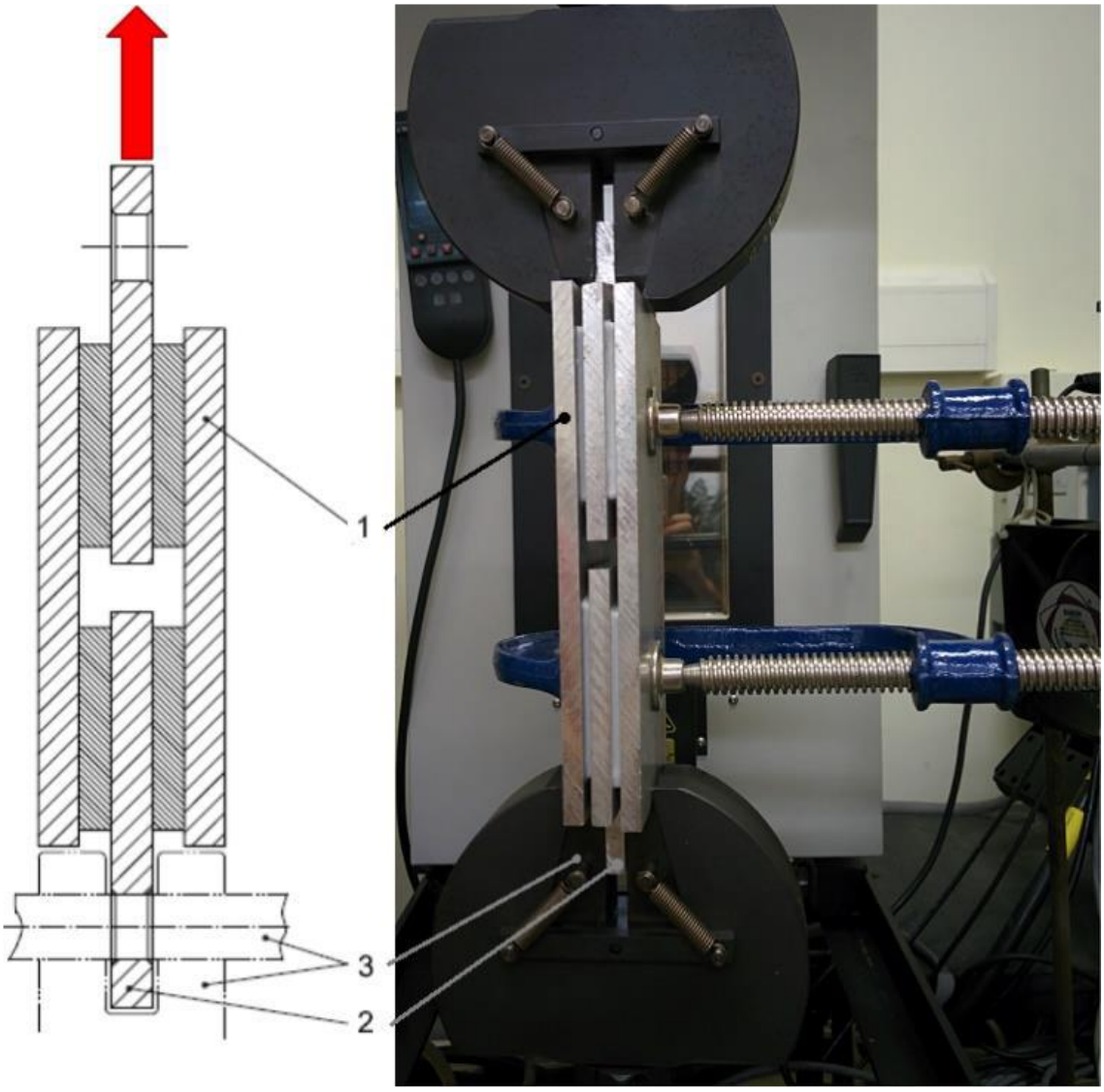

Figure 35. Schematic diagram of sample holder [24]and measurement setup, (1) – two external plates, (2) – two internal plates and (3) fixture for tensile loading.

Before the commerce of the test, a mechanical conditioning procedure was required. Here, five successive shear-loading cycles from strain of 0 to 0.3 were employed before the measurements. In Figure 36, the shear stress-strain curves of eight successive shear-loading cycles show that mechanical conditioning procedure is necessary for the test to obtain consistent data, while the data become consistent from cycle 5 or more. Thus,

based on the results from Figure 36, we selected five successive shear-loading cycles in our pre-test conditioning procedure.

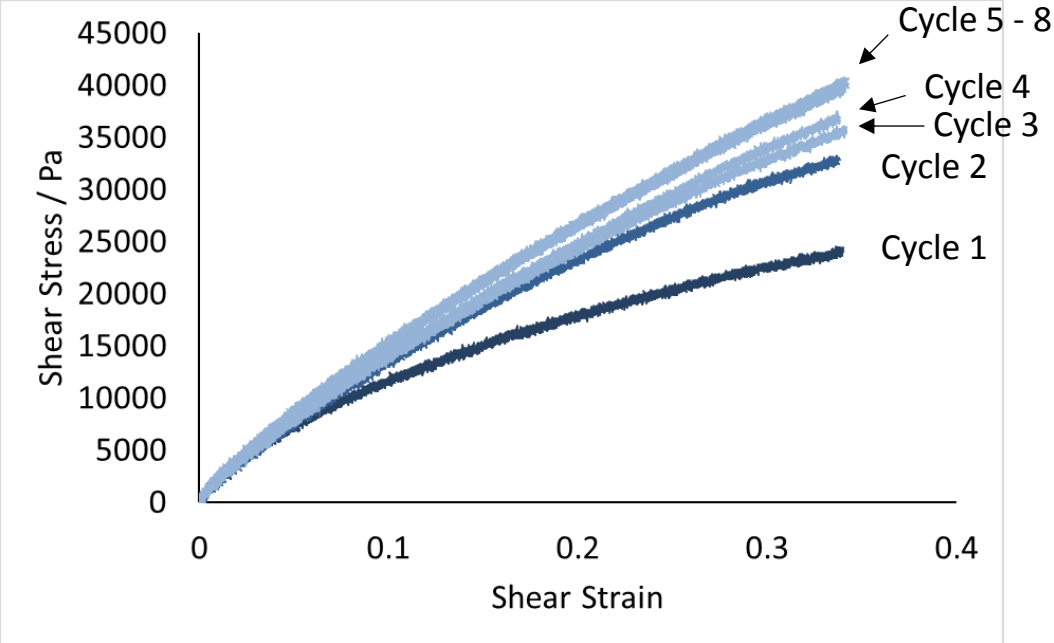

Figure 36. The shear stress-strain curves of eight successive shear-loading cycles

In order to obtain both lateral and vertical shear moduli, the vertical shear modulus was measured first, the samples were placed on the sample holder with the longest side paralleled to the applied force direction, then applied five cycles of shear-loading for mechanical conditioning and advanced three cycles for data record. Then the lateral modulus was measured, the samples were placed on the sample holder with the longest side perpendicular to the applied force direction, then applied five cycles of shear-loading for mechanical conditioning and advanced three cycles for data record. The samples arrangement can be referred in Figure 37.

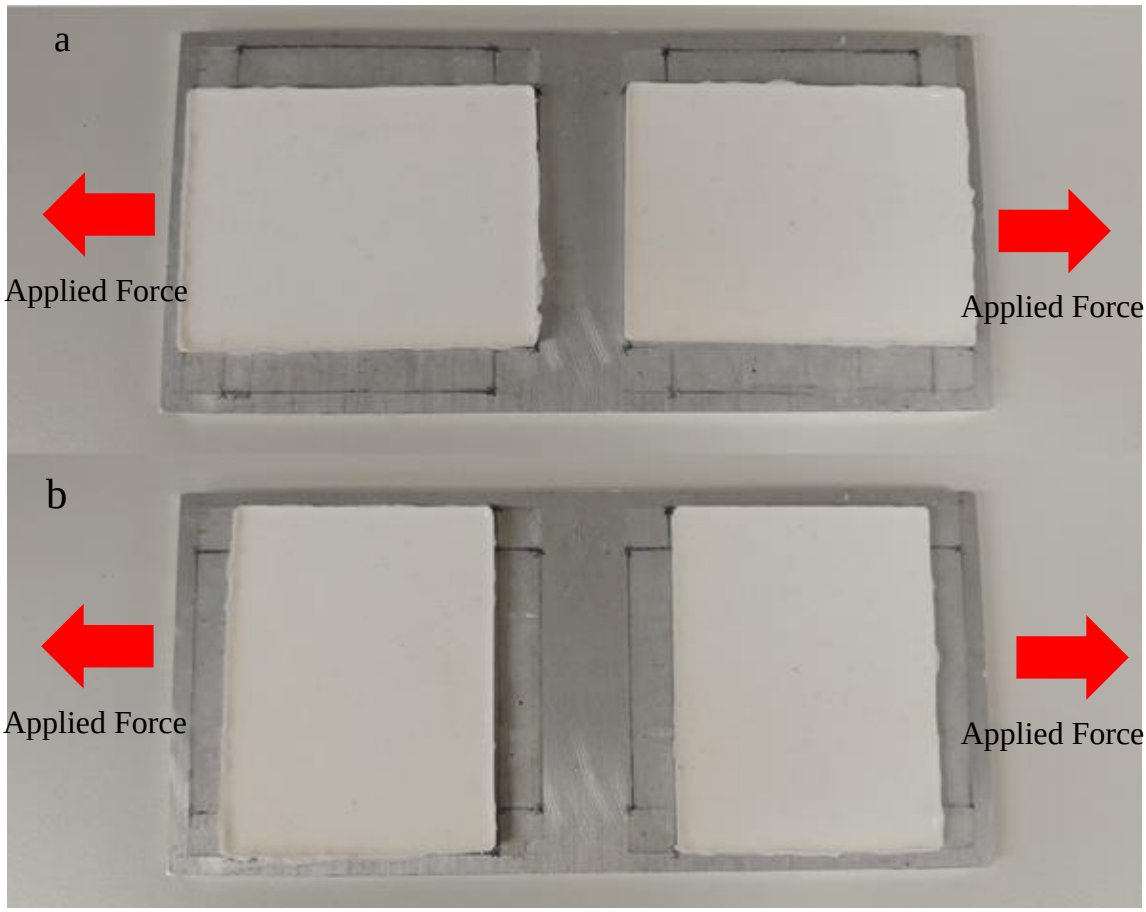

Figure 37. Samples arrangement in (a) vertical shear modulus (b) lateral shear modulus measurement

According to ISO1827, the shear modulus was determined at a shear strain of 0.25. Consider the measurement setup, the shear strain γ is given by

$$\gamma = \frac{d}{2c}$$ **Equation 15**

where d is the deformation of the sample

c is the thickness of the sample

The force needed to give 0.25 shear strain can be determined from the force/deformation curve. The shear stress at 0.25 strain, τ_{25}, is given by,

$$\tau_{25} = \frac{F_{25}}{2A}$$ **Equation 16**

where F_{25} is the applied force at shear stain of 0.25

A is the contact area between sample and rigid plate of one face of the sample

The shear modulus G is given by,

$$G = \frac{\tau_{25}}{\gamma_{25}} = \frac{\tau_{25}}{0.25}$$ **Equation 17**

The shear modulus is determined by the mean value for three measurements.

4.3.2. Measurement Results

For the glass fibre reinforced composite, no correlation between filing factor and shear moduli ratio is observed. Refer to Figure 38 and Figure 39, it is difficult to see any trend that between the filling factor and the shear moduli of the composite.

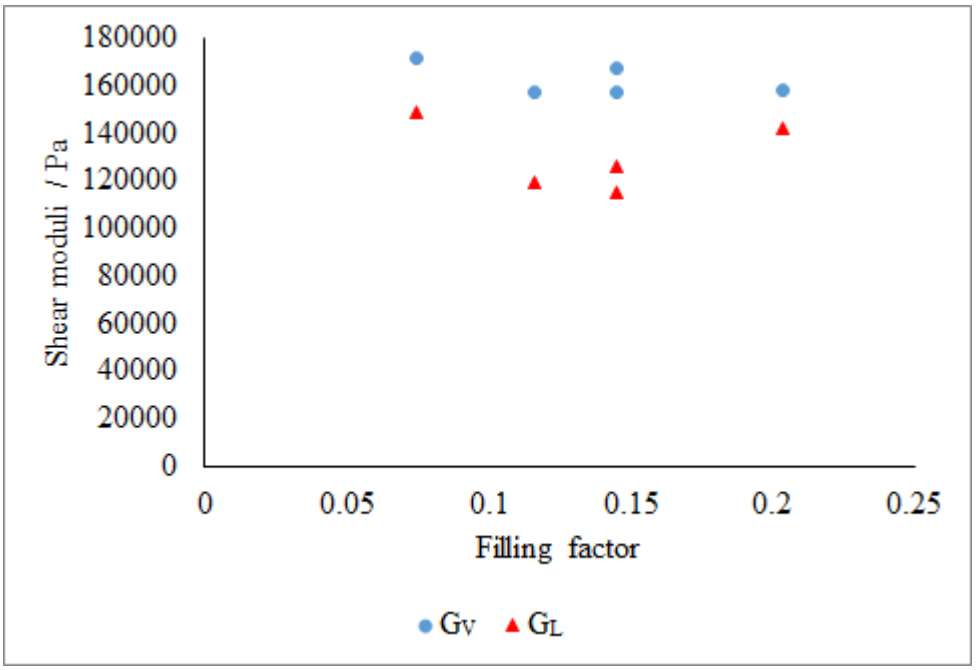

Figure 38. The graph of lateral and vertical shear moduli against filling factor of glass fibre reinforced composite by measurement

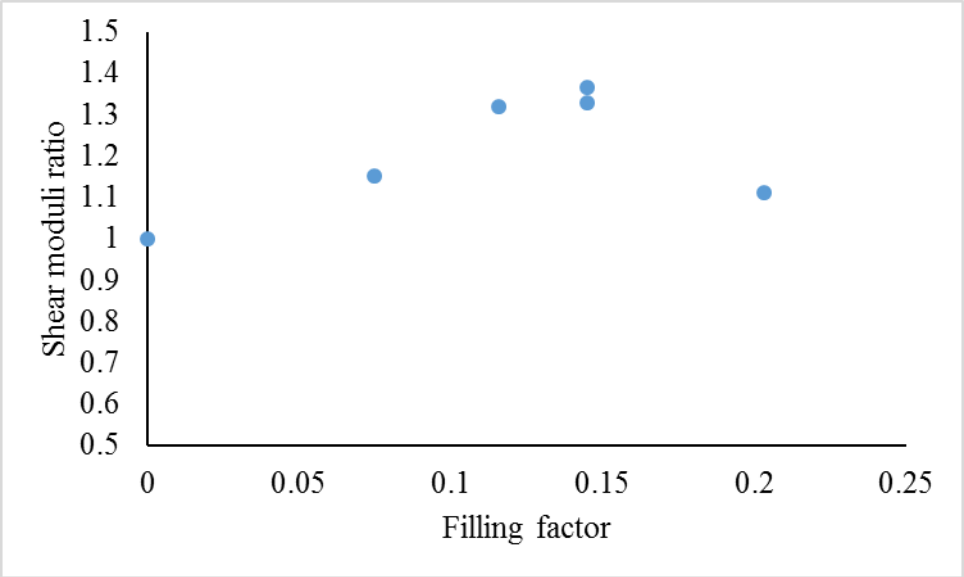

Figure 39. The graph of shear moduli ratio against filling factor of glass fibre reinforced composite by measurement

In Figure 39, the shear moduli ratio increases from filling factor of zero and reaches the maximum of 1.36 at 0.145, then the ratio starts to decreases.

The poor alignment and adhesion of the glass fibre might be the reason of the inconsistent of the glass fibre composite. The significant detachment was observed at filling factor of 0.145, which reaches the maximum shear moduli ratio.

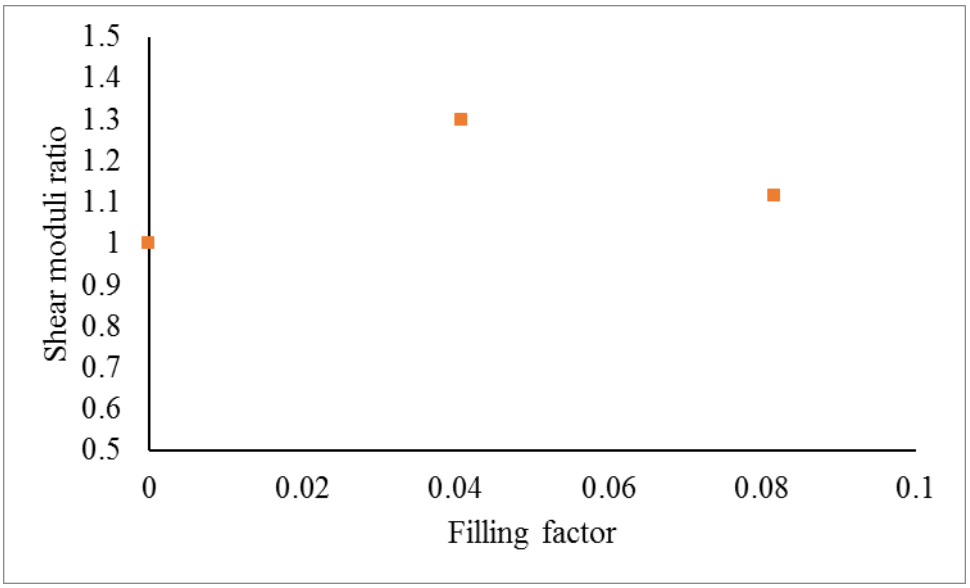

Figure 40. The graph of shear moduli ratio against filling factor of copper stripe reinforced composite by measurement

For copper stripe reinforced composite, the shear moduli ratio reaches 1.30 at filling factor of 0.04 and a lower ratio is found at filling factor of 0.08.

Copper stripe reinforced composite can obtain a comparable shear moduli ratio with lower filling factor than glass fibre reinforced composite.

4.4. Mechanical Properties of neoprene based composite

As mentioned in the former section, a neoprene rubber is preferable to be the matrix material in the study, due to the match of shear modulus to be used in the real TMD. However, the fabrication of the neoprene rubber requires a hydraulic heat press machine for the curing and the moulding process. Neoprene rubber is not able to be processed in laboratory due to the absence of heat press machine. Therefore, a set of four neoprene based steel stripe reinforced composite was provided by a manufacturer in mainland china, photos of a typical set of sample are shown in Figure 41. The composite was 72mm long, 54mm wide and 3mm thick, excluding the bulge part. There were 40 steel stripes erected

in the composite 72mm long, 2mm wide and 0.5mm thick, which has filling factor of 0.247. The neoprene rubber was in Shore hardness of 40A, which equals Young Modulus of 2.0GPa and Shear Modulus of 690kPa.

The mould used for neoprene based composite is different from the Teflon mould used for the glass fibre and copper stripes composite, it has reserved slots to erect and hold steel stripes in place during curing. The curing condition of the neoprene rubber was 210^{o}C for 180 seconds in the heat press machine.

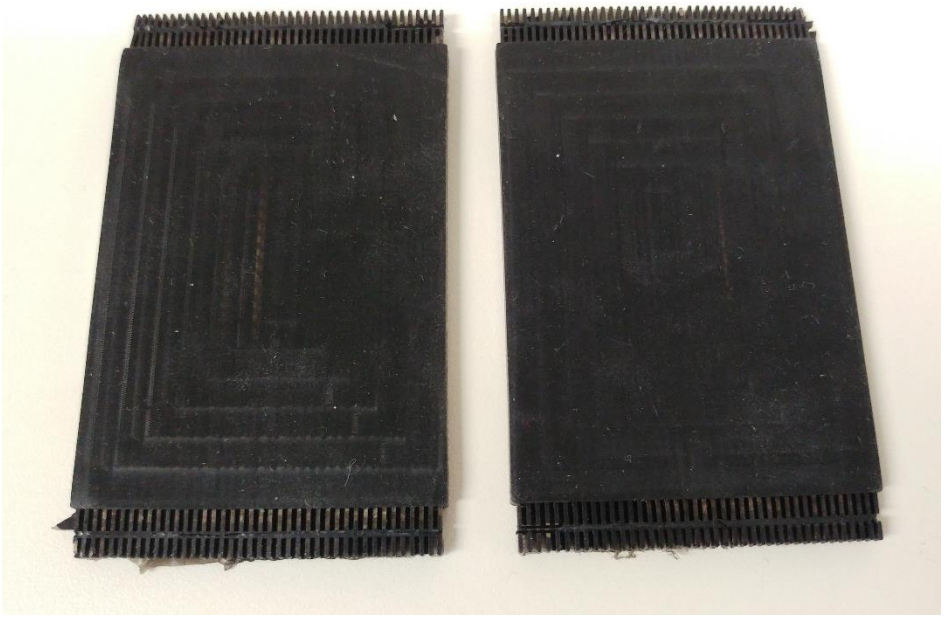

Figure 41. The photos of the neoprene based composite

The shear moduli measurement shows the neoprene composite has vertical shear modulus of 400kPa, lateral shear modulus of 357kPa and shear moduli ratio of 1.12.

4.5. Vibration Test of TMD

Apart from the shear moduli of the orthogonal resilient layer, there is a more direct method to evaluate the performance of the resilient layer. Using vibration test that deploys the resilient layer into a damper module, we can identify the resonance frequencies of the

oscillation mass along the lateral and vertical directions. In this section, the measurement setup and the results will be mentioned.

4.5.1. Measurement Setup

Through measuring the frequency responses due to impact along lateral and vertical directions, the resonance frequencies of the mass damper system along the lateral and vertical directions were identified. Figure 42 shows the measurement setup for the vibration test. According to the damper module design, the composite samples were deployed in two damper modules, which were between the oscillation mass and the segment plates which were fixed with screw and bolts. Two TMD modules were mounted on both sides of a UIC60 railtrack with 320mm long, instead of fixing the railtrack on sleepers, the railtrack with damper modules was hanged in order to avoid resonance from pinned-pinned modes and other sources.

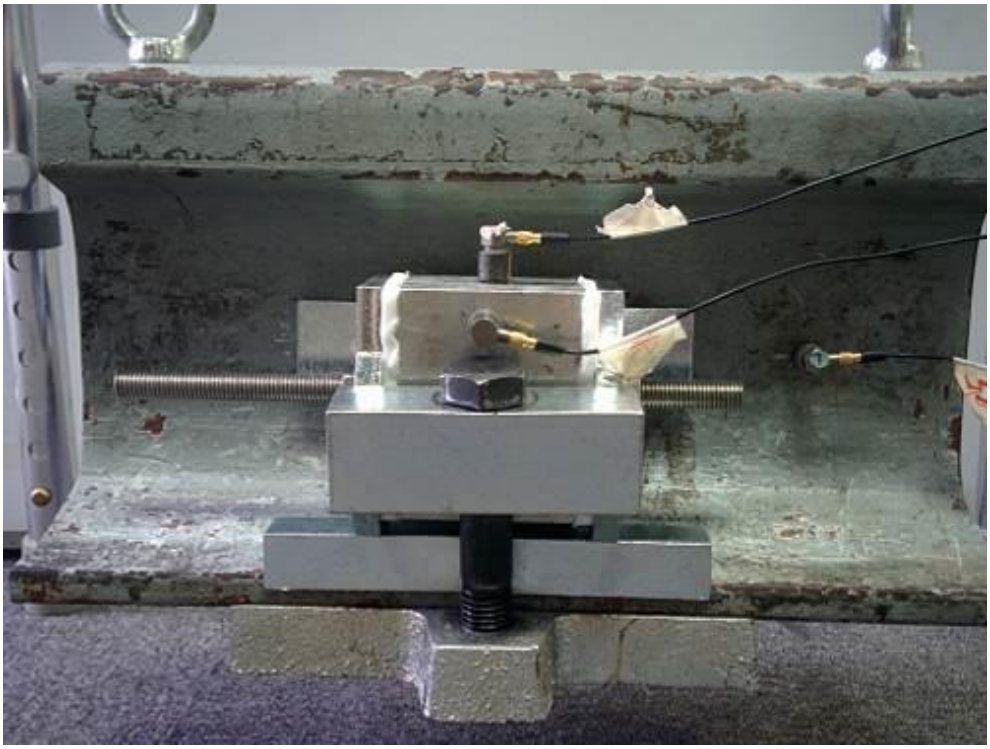

Figure 42. Measurement setup for vibration test

Three accelerometers in total were used to measure the magnitude of velocity. Two of them were placed on the oscillation masses of the two TMDs to monitor the vibration along either lateral or vertical directions, and one accelerometer was placed on rail as a reference and trigger to activate the data logger. A vertical impact to the railtrack excited a vibration on the railtrack and TMDs modules. The oscillation masses vibrated in their resonance frequencies and the impulse response was measured by the corresponding accelerometer sensors. Hence, studying the spectra of response can extract the resonance frequencies of the oscillation masses.

Figure 43 shows the schematic diagram of the impact points and position of accelerometer sensors. Here, accelerometer sensors V1 and V2 monitored vertical vibration while L1 and L2 monitored lateral vibration. The reference sensor was positioned accordingly at L Ref. for lateral test and V Ref. for vertical test. All spectra in the test were the results of the average of five impact responses.

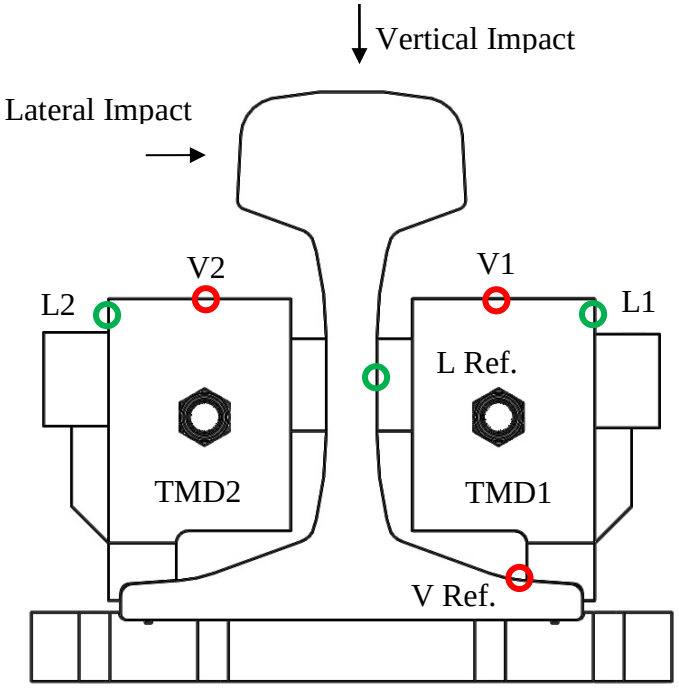

Figure 43. Schematic side view of the impact points and position of accelerometer on track

4.5.2. Measurement Results

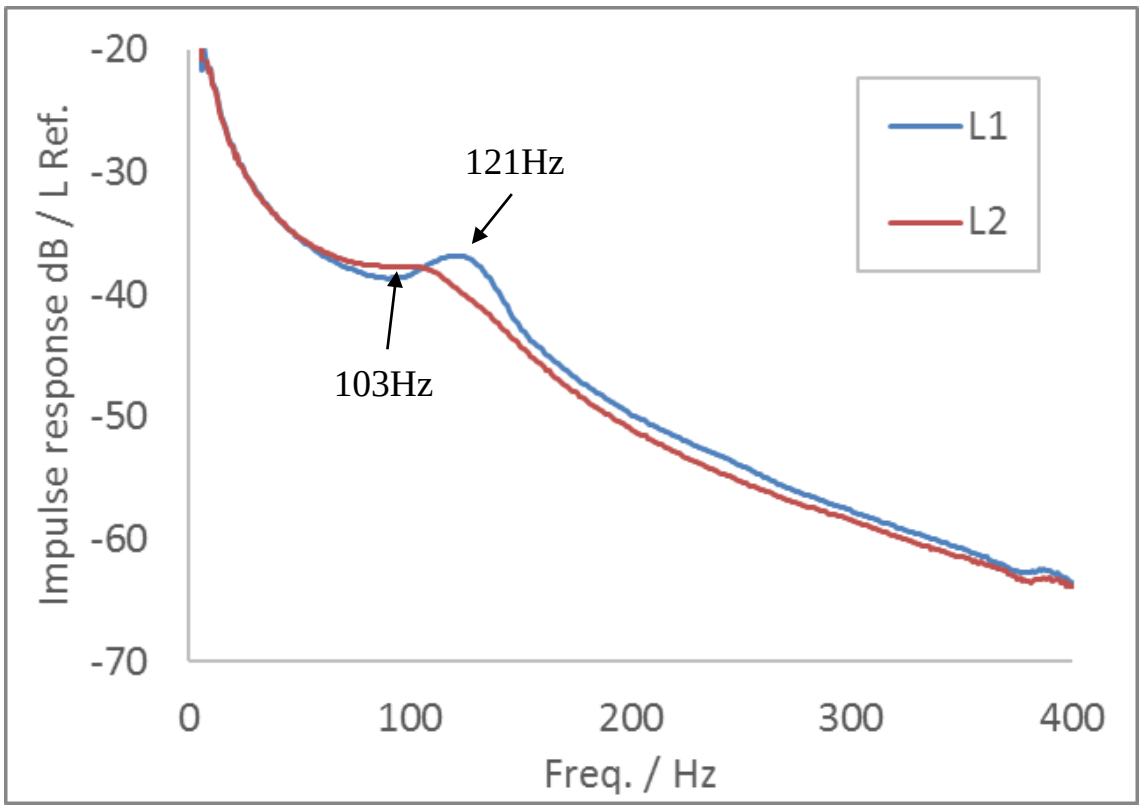

Figure 44. Impulse response spectrum in lateral test

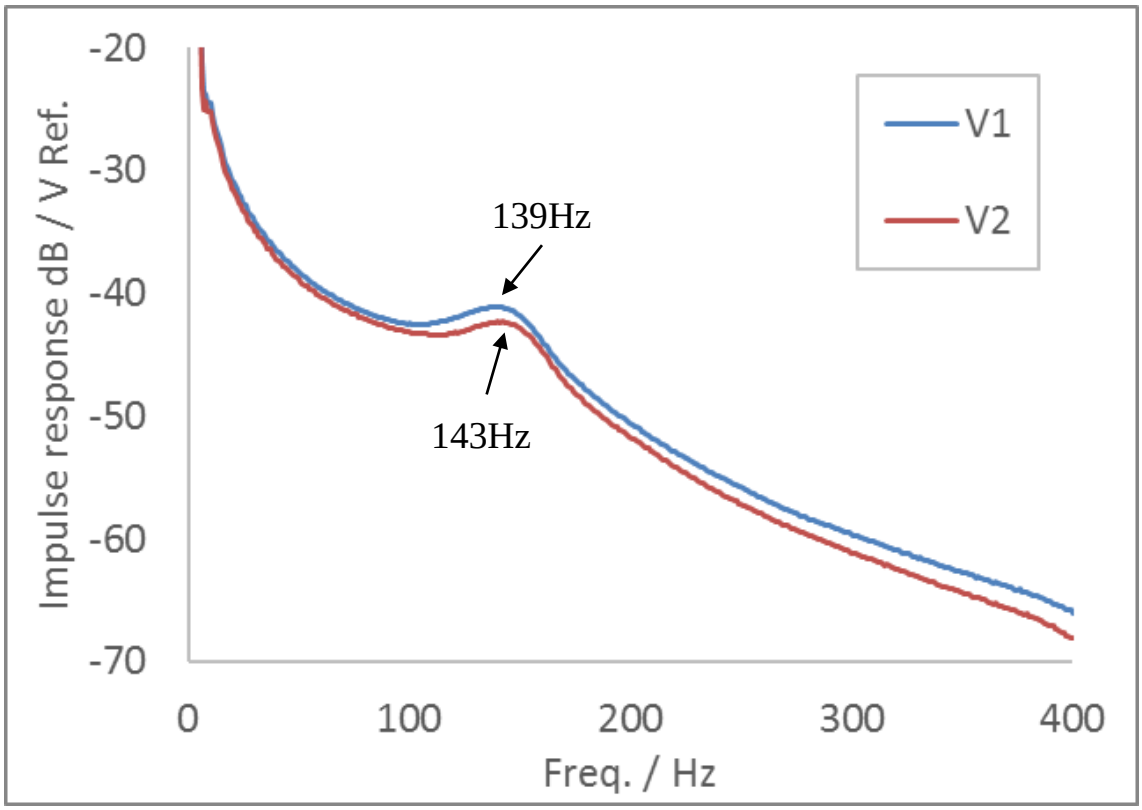

Figure 45. Impulse response spectrum in vertical test

As the impact is a single impulse, it can be considered with a period of infinite, which is 0Hz in frequency. Therefore, the impulse response is more favourable in low frequency region and the intensity of the impulse response decreases with the frequency, which makes an envelope for the response. When the tuned mass is vibrating in its resonance frequency, the vibration in such frequency would be more intense than other frequency, which means a peak shown in the envelope. The peak in frequency response indicates the resonance frequency of the corresponding tuned mass.

Figure 44 shows the frequency response curve in lateral direction. The oscillation masses have resonance frequencies at 121Hz and 103Hz in the lateral direction. The overall average is 112Hz.

Figure 45 shows the frequency response curve in vertical direction. The oscillation masses have resonance frequencies at 139Hz and 143Hz in the lateral direction, and the average is 141Hz.

The impulse response spectra indicate the presence of a clear frequency difference in two resonance modes for the same mass using orthogonal resilient layer. This frequency difference is not possible for resilient layer made by homogeneous materials.

The dispersion of our measured resonance frequencies of oscillation masses is probably due to the orthogonal resilient layer made by the composite developed in this thesis. Besides, the shear modulus measurement method can only obtain an averaged shear modulus for four test pieces. Although all four test pieces have the same configuration of fibre and matrix, individual variance is inevitable.

The glass fibre reinforced composite samples in this test has a shear moduli ratio of 1:1.34, thus, the resonance frequency ratio is expected to be 1:1.16 according to Equation 14. However, the frequency response test showed a ratio of 1:1.26 i.e. 141Hz / 112Hz = 1.26, which is slightly higher than the prediction from Equation 14.

Silicone is a viscoelastic material that has frequency-dependent properties during deformation. A higher frequency deformation on viscoelastic materials leads to a higher stiffness[25, 26]. This may provide a possible reason to the effect of deviated expectation of resonance frequency which is higher than expected. In such case, a viscoelasticity model should be introduced into consideration for high frequency damping.

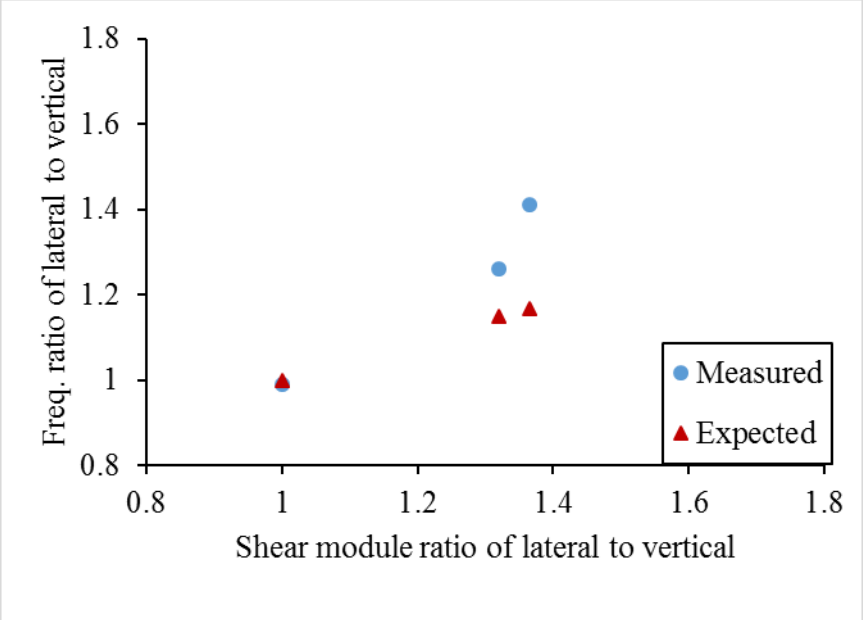

Figure 46. Frequency ratio along lateral to vertical directions against the corresponding shear modulus ratio

The resonance frequencies of three composite samples with known shear moduli ratios were measured through the vibration test. The results were plotted in Figure 46. For the sample with shear modulus ratio closed to one, the Equation 14 is still able to provide good prediction to the frequency ratio. As the shear moduli ratio increases, the measured frequency ratios become larger than those values obtained from the equation.

4.5.3. Study of the effect of Fastening Torque of TMD on resonance frequency

In this section, effect of the fastening torque of TMD on the resonance frequency is presented. According to the current design of TMD (see Figure 47), the damper modules that consists oscillation masses, resilient layer and segment plates were installed in series manner using screws and bolts. It is found that the fastening torque of the screws and bolts slight affects the resonance frequencies of the damper module from the experiments.

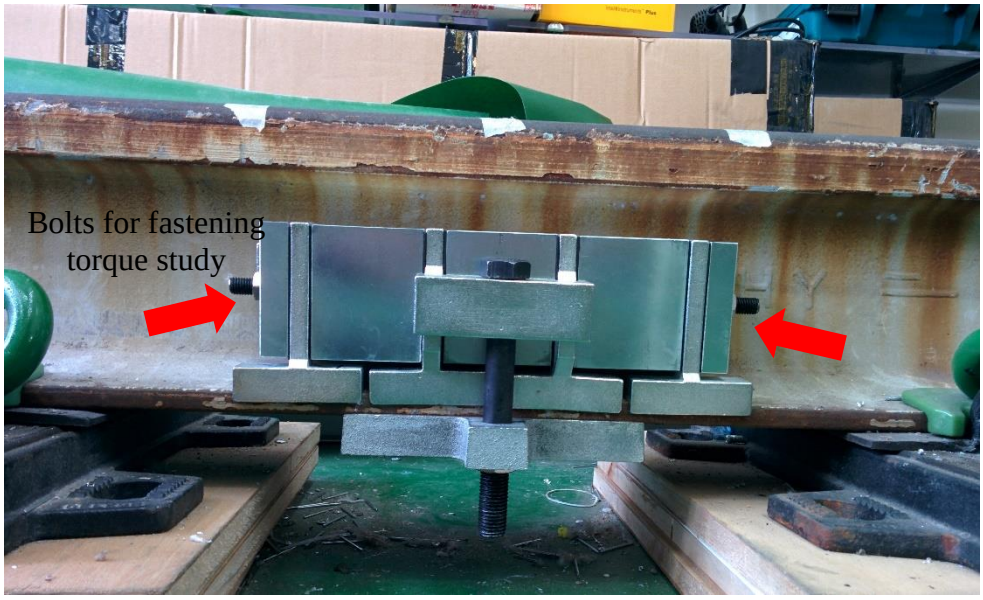

Figure 47. The side view of current design of TMD with located the bolts for fastening torque study

In our study, multiple vibration tests were conducted under different fastening torques which varied from 120kg-cm to 210kg-cm. Four oscillation masses were employed in the test, which are tuned desirable for 350Hz, 600Hz, 800Hz and 1.8kHz through different values of shear moduli of resilient layers.

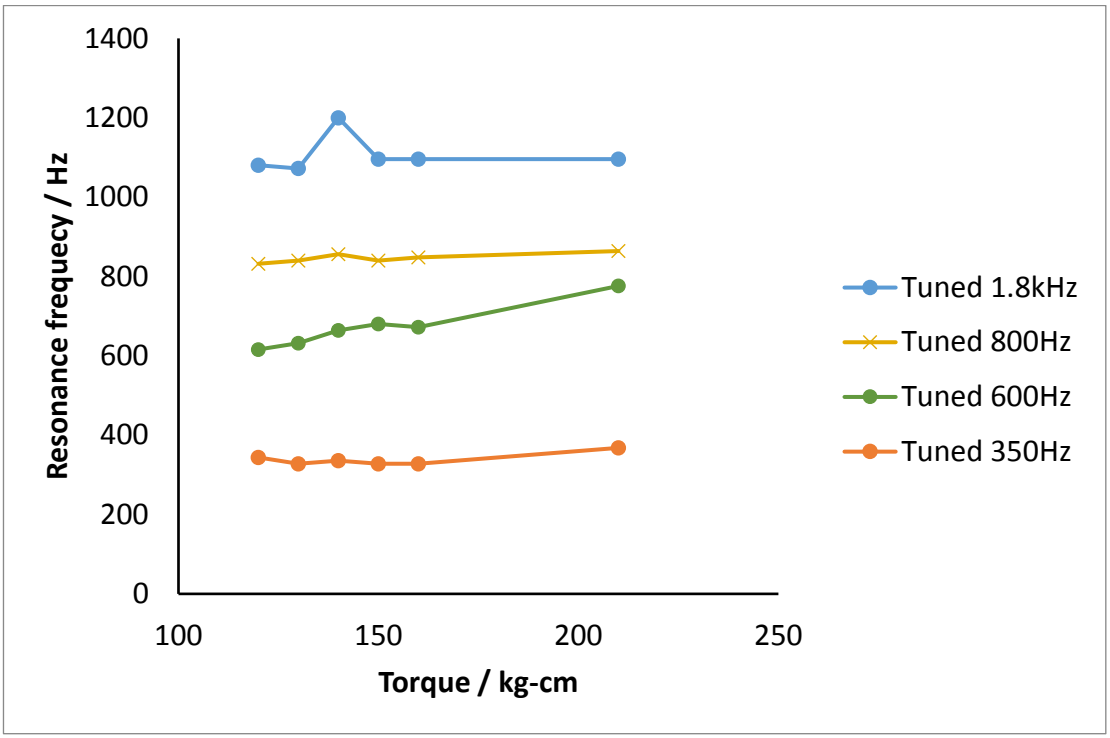

Figure 48. The graph of resonance frequency against fastening torque

In Figure 48, all masses show that the higher the applied fastening torque the higher the resonance frequency in results, although there a fluctuation of 1.8kHz mass is observed. The maximum difference located at 600Hz mass, which has an increase of 160Hz from 120kg-cm to 210kg-cm. This slightly adjustment can be applied to fine tune the final resonance frequency, while the resilient layer has deviated quality issue although the masses in whole damper module will also be affected.

As the fastening torque directly affects the clamping pressure between the segment plates, resilient layers and oscillation mass, the resilient layers will be subjected to a pressure that induces a strain to the resilient layers. This strain acted as a pre-strain to the material. A higher magnitude of force is required to make the same amount of deformation for a pre-strain material, which leads an equivalent higher elastic modulus for the material.

5. Conclusion

Pinned-pinned resonance modes on the railtrack produce rolling noise and corrugation on the running surface of the rail, one of the mitigations is installation of railtrack tuned mass damper, while the masses can be tuned to a desired resonance frequency to limit the vibration displacement of the railtrack. The pinned-pinned resonance modes of the railtrack in lateral and vertical direction are in the frequency ratio of around 1:2, which means two oscillation masses needed to be deployed to handle pinned-pinned modes for conventional TMD. To fully utilize the limited space along the railtrack and spare oscillation masses for other desired frequencies, an orthogonal resilient material is suggested to deploy in the current design of TMD.

A computation model using FEA was developed to study the shear moduli of copper stripes reinforced neoprene composite in various configurations. The results suggest that the maximum shear moduli ratio reaches 2.03 at filling factor of 0.06.

The two types of orthogonal composites were fabricated and tested for the application, they are glass fibre reinforced composite and copper stripes reinforced composite. Their relationship fibre configuration and shear moduli were studied. Glass fibre reinforced composite can reach shear moduli of 1.36 and copper stripe reinforced composite of 1.30. A neoprene rubber based composite was fabricated by a manufacturer in mainland, and the orthogonal shear moduli were also measured. The shear moduli ratio reaches 1.12.

The fundamental concepts of the orthogonal resilient materials have been confirmed through the vibration test showing that the damper module with composite resilient layer

is capable to have two resonance modes in two orthogonal directions, which is not possible to achieve for homogeneous materials.

Furthermore, the ability of fine tuning resonance frequency of the damper module through adopting different fastening torque of bolts was briefly studied.

To further improve the tuned mass damper modules, there are three crucial future works should be considered and achieved. First, the composite configuration that reaches a higher shear moduli ratio should be found, since the resilient layers are required to have a shear stiffness ratio of about 1:4 to handle the orthogonal vibration in frequency ratio of about 1:2. Second, the composite materials should have high weather resistance. As the composite is designated to be deployed outdoor during normal operation, the composite should be weather resist and preserves its elastic properties disregard the weather factors. Third, the materials selected for the orthotropic composite should be suitable for mass-production, as the tuned mass damper module will be installed between every sleeper over the railtrack to reduce rolling noise. For example, a 100m long railtrack section with sleeper separation of 0.7m, 284 tuned mass damper modules will be installed, which needs 4544 of resilient layers deployed in those damper modules. A mass production of composite will be a certain.

Reference

[1] D. Thompson, *Railway noise and vibration: mechanisms, modelling and means of control*: Elsevier, 2008.
[2] W. Ho, B. Wong, D. England, and A. Pang, "Tuned mass damper for rail noise and corrugation control," *Acoustics 2012*, 2012.
[3] W. Ho, B. Wong, D. England, A. Pang, and C. To, "Reduction of corrugation growth rate by rail dampers," *TDHRail Magazine*, vol. 47, pp. 18-19, 2013.
[4] S. Grassie, "Rail corrugation: characteristics, causes, and treatments," *Proceedings of the Institution of Mechanical Engineers, Part F: Journal of Rail and Rapid Transit*, vol. 223, pp. 581-596, 2009.
[5] ISO, "Mechanical vibration and shock — Experimental determination of mechanical mobility " in *Part 1: Basic terms and definitions, and transducer specifications* vol. ISO 7626, ed, 2011.
[6] W. Ho, T. Cai, and B. Wong, "Analytical study on railway corrugation growth control by tuned mass damper," in *The 21st International Congress of Sound and Vibration*, 2014.
[7] J. Connor and S. Laflamme, *Structural motion engineering*: Springer, 2014.
[8] J. P. Den Hartog, *Mechanical vibrations*, 4th ed. New York: McGraw-Hill, 1956.
[9] E. Madenci and I. Guven, "The finite element method and applications in engineering using ANSYS®," Second edition. ed. New York: Springer, 2015.
[10] C.-C. Lin and J.-F. Wang, "Optimal design and practical considerations of tuned mass dampers for structural control," *Design Optimization of Active and Passive Structural Control Systems*, 2012.
[11] H. Kitamura, T. Fujita, T. Teramoto, and H. Kihara, "Design and analysis of a tower structure with a tuned mass damper," in *Proceedings 9th World Conference of Earthquake Engineering, Tokyo-Kyoto, Japan*, 1988, pp. 415-420.
[12] (1976) Lead hula-hoops stabilize antenna. *Engineering News Record*.
[13] R. J. McNamara, "Tuned mass dampers for buildings," *Journal of the Structural Division*, vol. 103, pp. 1785-1798, 1977.
[14] N. R. Petersen, "Design of large scale tuned mass dampers," *Structural control*, pp. 581-596, 1980.
[15] T. Nagase and T. Hisatoku, "Tuned pendulum mass damper using ice thermal storage tank installed in crystal tower," *Private Communication*, 1990.
[16] P. Irwin, J. Kilpatrick, J. Robinson, and A. Frisque, "Wind and tall buildings: negatives and positives," *The structural design of tall and special buildings*, vol. 17, pp. 915-928, 2008.
[17] K. K. Chawla, *Composite materials: science and engineering*: Springer Science & Business Media, 2012.
[18] E. J. Barbero, *Finite element analysis of composite materials using ANSYS®*: CRC press, 2013.
[19] K.-J. Bathe, *Finite element procedures in engineering analysis*. Englewood Cliffs, N.J: Prentice-Hall, 1982.
[20] M. Ohring, *Engineering Materials Science*. San Diego: Academic Press, 1995.
[21] R. W. Ogden, *Non-linear elastic deformations*: Courier Corporation, 1997.

[22] E. P. DeGarmo, J. T. Black, R. A. Kohser, and B. E. Klamecki, *Materials and process in manufacturing*: Prentice Hall, 1997.

[23] J. M. Holt, H. Mindlin, and C. Y. Ho, *Structural alloys handbook*: CINDAS/Purdue University, 1994.

[24] ISO, "Rubber, vulcanized or thermoplastic — Determination of shear modulus and adhesion to rigid plates — Quadruple-shear methods," ed, 2011.

[25] A. J. Goldberg, "Viscoelastic properties of silicone, polysulfide, and polyether impression materials," *Journal of dental research*, vol. 53, pp. 1033-1039, 1974.

[26] M. T. Shaw and W. J. MacKnight, *Introduction to polymer viscoelasticity*: John Wiley & Sons, 2005.